Cell Reports

Article

Stem cell plasticity, acetylation of H3K14, and *de novo* gene activation rely on KAT7

Graphical abstract

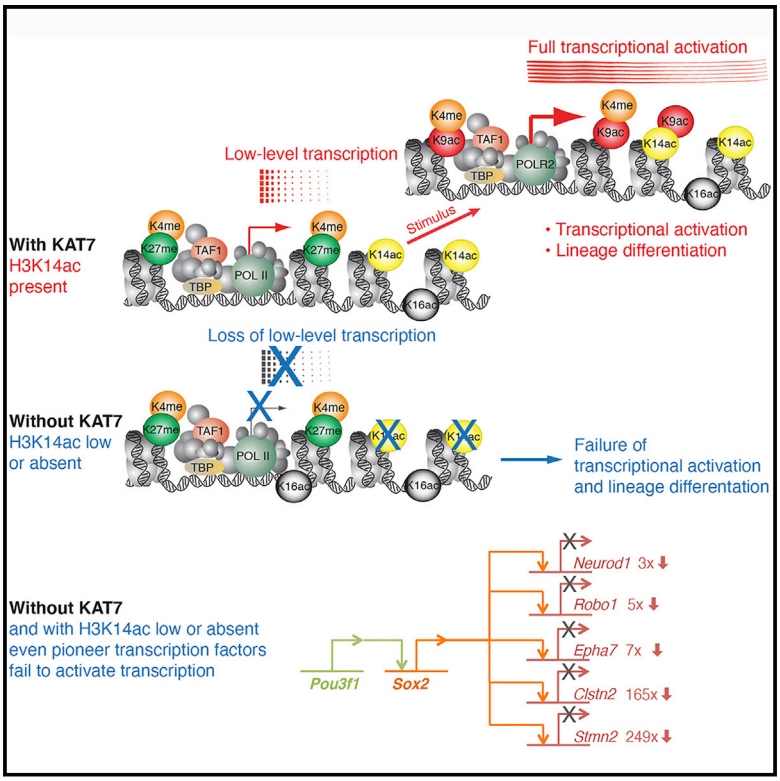

Highlights

- KAT7 is essential for H3K14 acetylation, neuron, and oligodendrocyte differentiation
- KAT7 and H3K14ac are distributed widely in the genome, including in H3K9me3+ domains
- Neuronal gene expression program fails to be activated in the absence of KAT7
- KAT7 creates a permissive chromatin state for transcriptional activation

Authors

Andrew J. Kueh, Maria I. Bergamasco, Anna Quaglieri, ..., Terence P. Speed, Tim Thomas, Anne K. Voss

Correspondence

tthomas@wehi.edu.au (T.T.), avoss@wehi.edu.au (A.K.V.)

In brief

The role of acetylation of specific histone lysine residues remains unclear. Kueh et al. find that the absence of the lysine acetyltransferase KAT7 in neural stem cells causes loss of H3K14 acetylation, a failure to activate the neuron differentiation gene expression program, and neuronal differentiation.

Kueh et al., 2023, Cell Reports *42*, 111980
January 31, 2023
https://doi.org/10.1016/j.celrep.2022.111980

CellPress

Cell Reports

CellPress
OPEN ACCESS

Article

Stem cell plasticity, acetylation of H3K14, and *de novo* gene activation rely on KAT7

Andrew J. Kueh,[1,2,6] Maria I. Bergamasco,[1,2,6] Anna Quaglieri,[1] Belinda Phipson,[1,2,3] Connie S.N. Li-Wai-Suen,[1,2] Ingrid M. Lönnstedt,[1] Yifang Hu,[1] Zhi-Ping Feng,[1] Chris Woodruff,[1] Rose E. May,[1] Stephen Wilcox,[1] Alexandra L. Garnham,[1,2] Michael P. Snyder,[4] Gordon K. Smyth,[1,5] Terence P. Speed,[1,5] Tim Thomas,[1,2,7,*] and Anne K. Voss[1,2,7,8,*]

[1]Walter and Eliza Hall Institute of Medical Research, Melbourne, VIC 3052, Australia
[2]Department of Medical Biology, The University of Melbourne, Melbourne, VIC 3052, Australia
[3]Department of Paediatrics, The University of Melbourne, Melbourne, VIC 3010, Australia
[4]Department of Genetics, Stanford University School of Medicine, Stanford, CA 94305, USA
[5]School of Mathematics and Statistics, University of Melbourne, Melbourne, VIC 3010, Australia
[6]These authors contributed equally
[7]These authors contributed equally
[8]Lead contact
*Correspondence: tthomas@wehi.edu.au (T.T.), avoss@wehi.edu.au (A.K.V.)
https://doi.org/10.1016/j.celrep.2022.111980

SUMMARY

In the conventional model of transcriptional activation, transcription factors bind to response elements and recruit co-factors, including histone acetyltransferases. Contrary to this model, we show that the histone acetyltransferase KAT7 (HBO1/MYST2) is required genome wide for histone H3 lysine 14 acetylation (H3K14ac). Examining neural stem cells, we find that KAT7 and H3K14ac are present not only at transcribed genes but also at inactive genes, intergenic regions, and in heterochromatin. KAT7 and H3K14ac were not required for the continued transcription of genes that were actively transcribed at the time of loss of KAT7 but indispensable for the activation of repressed genes. The absence of KAT7 abrogates neural stem cell plasticity, diverse differentiation pathways, and cerebral cortex development. Re-expression of KAT7 restored stem cell developmental potential. Overexpression of KAT7 enhanced neuron and oligodendrocyte differentiation. Our data suggest that KAT7 prepares chromatin for transcriptional activation and is a prerequisite for gene activation.

INTRODUCTION

Stem cells must maintain their own cell identity and undergo self-renewing cell divisions, while retaining the capacity to differentiate into morphologically and functionally distinct progeny. Neural stem cells of the forebrain can give rise to neurons, astrocytes, and oligodendrocytes,[1,2] mirroring the tightly choreographed proliferation and differentiation of neuronal cells during embryogenesis and fetal development. Cell fate changes necessitate silencing of stem cell-specific genes and activation of the new expression programs. These processes are accompanied by modifications of the chromatin.[3–5] Chromatin-mediated repression needs to be overcome[6] in order to induce new gene expression programs. Pioneer transcription factors, which have the unique ability to bind their full or partial response element while the DNA is wrapped around nucleosomes, are thought to initiate conversion of repressed chromatin to transcriptionally active chromatin.[7] The pioneer transcription factors SOX2,[8,9] NEUROD,[10] and ASCL1[11] are required in the neuronal lineage. Activation of the neuronal program further requires the transcription factors POU3F1 and PAX6,[12–15] and the oligodendrocytic program includes OLIG1 and OLIG2.[16,17]

Chromatin requirements prior to the process of initiation of a new gene expression program, if any, are poorly understood. Genome-wide studies suggested a general association of histone acetylation[18] and acetyltransferases[19] with active gene transcription. However, the molecular and cellular effects of individual histone acetylation marks in mammals have remained elusive, possibly for two reasons: the multitude of functionally overlapping histone genes in the mammalian genome has precluded studies of point mutations of specific histone residues and the reported substrate lysine promiscuity of lysine acetyltransferases based on biochemical activity in cell-free assays. In many cases it is unclear if posttranslational histone modifications are a cause or a consequence of gene transcription.[20] Moreover, the functional hierarchy of transcription factors and chromatin-modifying enzymes can be difficult to determine. Transcription factors recruit co-activators (e.g., Bertero et al.[21] and Lee et al.,[22]), but chromatin-modifying enzymes and their protein complex partners typically contain multiple chromatin binding domains that bind specific posttranslational histone modifications (reviewed in Lee and Workman[23]) and regulate the access of transcription factors to the DNA.[24,25] Thus, transcription factors and chromatin-modifying enzymes form an

interacting network in which primary and secondary events in establishing gene expression patterns are difficult to separate.[26]

KAT7 is a MYST (MOZ, YBF2/SAS3, SAS2, TIP60) family lysine acetyltransferase and was first named *histone acetyltransferase binding to the origin of replication complex protein 1* (HBO1), due to a fraction of the total KAT7 protein immuno-precipitating with the origin of replication complex.[27,28] Further studies supported a role in DNA replication.[29–32] Other studies suggest a primary role in transcriptional regulation.[33–36] KAT7 is the enzymatic component of protein complexes formed with EAF6 and the scaffold proteins ING4/5 and JADE1/2/3 or BRPF1/2/3, which contain bromo- and PHD chromatin binding domains.[29,37] Some reports suggest that KAT7 catalyzes acetylation of histones H3 and H4 either in cell-free assays or in HEK293T cells.[28,29,37–39] Other studies support the notion that KAT7 predominantly acetylates histone H3 on lysine 14 (H3K14) in mouse embryos and fibroblasts,[33] erythroblasts,[34] lung epithelial cells,[40] and human acute myeloid leukemia cells,[41] HeLa,[42–44] MCF7, and HEK293T cells.[44] A global reduction in H3K14ac was also observed in *Kat7* deleted mouse blood vessel endothelial cells,[45] bone marrow,[35] and T cells.[46] H3K14ac has been correlated with transcriptionally active genes in yeast and mammalian cells.[47–52]

Here we determined the requirement for KAT7 for histone acetylation, gene transcription, proliferation, cell fate commitment, and differentiation in the developing brain and neural stem and progenitor cells (NSPCs) after conditional deletion of the *Kat7* gene. In wild-type cells, KAT7 and H3K14ac were present throughout the genome. Deletion of the *Kat7* gene in NSPCs resulted in the loss of H3K14ac. *Kat7*-deleted NSPCs failed to differentiate into neurons and oligodendrocytes. KAT7 was required for the activation of the neuronal and oligodendrocytic gene expression programs from the uncommitted, repressed state. In the absence of KAT7, gene activation was insufficient or failed entirely and cell fate changes were effectively blocked.

RESULTS

Kat7-deleted NSPCs fail to differentiate into neurons and oligodendrocytes

We isolated $Kat7^{lox/lox}NesCre^{T/+}$ (*Kat7* deleted) and $Kat7^{+/+}NesCre^{T/+}$ (*Kat7* intact, control) E14.5 forebrain NSPCs. KAT7 protein was expressed in control cells and lost in $Kat7^{lox/lox}NesCre^{T/+}$ NSPCs (Figure 1A). NSPCs of both genotypes were readily propagated *in vitro* as floating colonies (neurospheres) and expressed NSPC marker proteins, including SOX2, nestin, and GFAP (Figure 1B) at levels per cell that were similar between genotypes (Figures S1 and S2). As expected, neural stem cells share the GFAP marker with astrocytes (summarized by Götz et al.[53]). NSPCs of both genotypes were successfully propagated for 15 passages (105 days; Figure 1C). However, over the period of this long-term culture, $Kat7^{lox/lox}NesCre^{T/+}$ cells accumulated more slowly than control cells (Figure 1C).

To test the developmental potential of NSPCs lacking KAT7, NSPCs were subjected to differentiation conditions for 1 to 7 days, and their ability to differentiate into neurons (βIII-tubulin$^+$), astrocytes (GFAP$^+$), and oligodendrocytes (O4$^+$) was examined. As assessed by morphology and marker protein expression, unlike $Kat7^{+/+}NesCre^{T/+}$ control NSPCs, $Kat7^{lox/lox}NesCre^{T/+}$ NSPCs were completely unable to form neurons and oligodendrocytes, but were able to form astrocytes (Figures 1D, S3 and S4). Assessment by flow cytometry confirmed that neuronal (βIII-tubulin$^+$) and oligodendrocyte (O4$^+$) differentiation were affected by the loss of KAT7, whereas astrocyte differentiation (S100β$^+$) proceeded normally (Figure 1E). In the later phase of differentiation, the median fluorescence intensity per cell, representing protein levels, for S100β was strongly increased in both genotypes. However, protein levels per cell for SOX2, GFAP, S100β, and βIII-tubulin appeared to be reduced in $Kat7^{lox/lox}NesCre^{T/+}$ compared with $Kat7^{+/+}NesCre^{T/+}$ control cells, suggesting that KAT7 continues to be important for the expression of differentiation markers throughout differentiation (Figure S2).

Kat7-deleted NSPCs can proliferate and self-renew but are susceptible to cell death

NSPCs can be propagated in culture as colonies (neurospheres) that contain NSPCs. Individual neurospheres were indistinguishable in size between genotypes early after the previous passage, namely day 3 after passage, but the $Kat7^{lox/lox}NesCre^{T/+}$ neurospheres displayed a reduction in size later in the passage interval (day 6 and day 9; Figure 2A).

Staining for the mitosis marker histone H3 phosphorylated on serine 10 (H3S10p) revealed that the proportion of cells in mitosis did not differ between genotypes early within each passage interval (day 3 after passage 5 or passage 10), suggesting that cell cycle progression was normal. However, the H3S10p positive proportion of cells was reduced in the $Kat7^{lox/lox}NesCre^{T/+}$ cultures later (day 6) within each passage interval, suggesting a problem with cell growth at these later stages (assessment after passage 5 or passage 10; Figures 2B and S5). Likewise, the number of secondary neurospheres generated by identical numbers of NSPCs plated after passage was similar in the two genotypes when the assay was performed early after the previous passage (day 3) but reduced in the $Kat7^{lox/lox}NesCre^{T/+}$ cultures at day 6 after the previous passage (assessment after passage 5 or passage 10; Figures 2C and S5). Flow cytometric analysis showed that the percentage of SOX2$^+$GFAP$^+$ cells representing stem cells was similar between genotypes early in the passage interval (day 3) but reduced later in the passage interval in $Kat7^{lox/lox}NesCre^{T/+}$ compared with control cultures (day 6; Figures 2D, S1 and S2). In contrast, the percentage of SOX2$^-$S100β$^+$ astrocytes was increased late in the passage interval in $Kat7^{lox/lox}NesCre^{T/+}$ cultures (Figure 2D). The percentage of live cells was decreased slightly early and substantially decreased late in the passage interval in $Kat7^{lox/lox}NesCre^{T/+}$ cultures compared with controls (Figure 2E). TUNEL$^+$ dead cells were increased in the $Kat7^{lox/lox}NesCre^{T/+}$ as compared with $Kat7^{+/+}NesCre^{T/+}$ control cultures (Figures 2E and S5).

These data show that NSPCs lacking KAT7 can proliferate at a constant rate, albeit slower than control cells, indicating that they do not exhaust their proliferation capacity over time. *Kat7*-deleted NSPCs formed secondary neurospheres normally in the first half of each cell culture passage interval, but as colony size increases, they show a reduction in secondary neurosphere formation, an increased level of cell death and an increase in astrocyte differentiation. The discrepancy between

CellPress
OPEN ACCESS

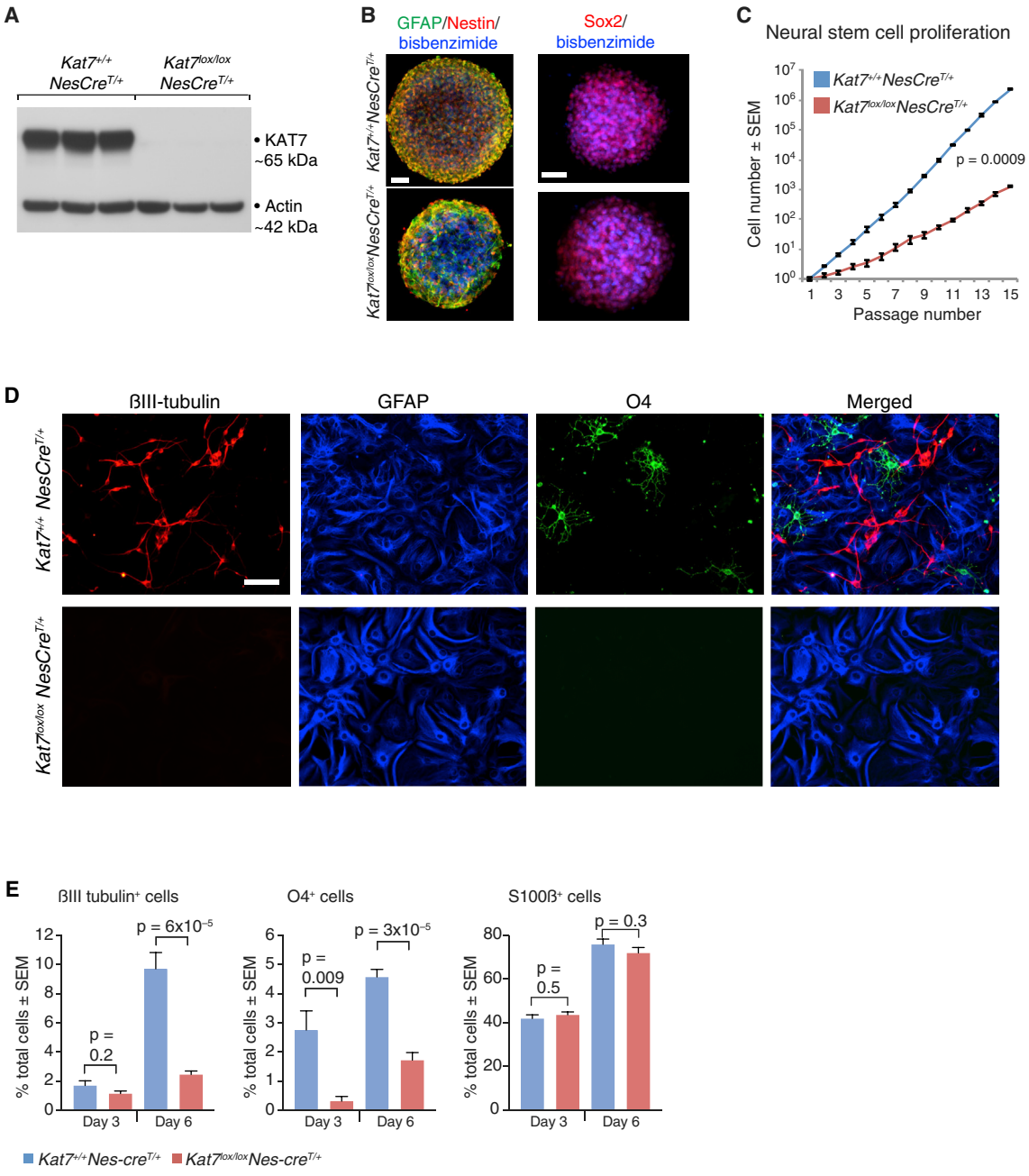

Figure 1. *Kat7*-deleted NSPCs proliferate but fail to differentiate into neurons and oligodendrocytes

(A) Immunoblot of KAT7 protein in total protein lysates of passage 5 *Kat7*$^{lox/lox}$*NesCre*$^{T/+}$ and *Kat7*$^{+/+}$*NesCre*$^{T/+}$ NSPC cultures. β-actin serves as loading control. Each lane represents cells isolated from one animal, i.e., n = 3 animals per genotype.

(B) Immunofluorescence staining for NSPC marker proteins nestin (red), GFAP (green), and SOX2 (red), and bisbenzimide nuclear counterstain (blue) in passage 5 *Kat7*$^{lox/lox}$*NesCre*$^{T/+}$ and *Kat7*$^{+/+}$*NesCre*$^{T/+}$ neurospheres. Scale bar indicates 48 μm.

(C) Growth of *Kat7*$^{lox/lox}$*NesCre*$^{T/+}$ and *Kat7*$^{+/+}$*NesCre*$^{T/+}$ NSPCs over 15 passages (105 days).

(D) *Kat7*$^{+/+}$*NesCre*$^{T/+}$ NSPCs give rise to type III ß-tubulin-positive neurons (red), GFAP-positive astrocytes (blue), and O4-positive oligodendrocytes (green), each with cell-type-specific morphology, when cultured under differentiation conditions (on laminin with 1% fetal bovine serum [FBS], without fibroblast growth factor 2 [FGF2], without epidermal growth factor [EGF]). In contrast, *Kat7*$^{lox/lox}$*NesCre*$^{T/+}$ NSPCs fail to form neurons and oligodendrocytes and only form astrocytes. Scale bar, 80 μm. A time course of differentiation is shown in Figures S3 and S4.

(E) Flow cytometric assessment of neurons (βIII-tubulin$^+$), oligodendrocytes (O4$^+$), and astrocytes (S100β$^+$) as percentage of live cells in cultures of differentiating *Kat7*$^{lox/lox}$*NesCre*$^{T/+}$ and *Kat7*$^{+/+}$*NesCre*$^{T/+}$ NSPCs. Flow cytometry gating strategy and median fluorescence intensities are shown in Figures S1 and S2.

Experiments were conducted on passage 5 proliferating NSPCs (A, B) or NSPCs induced to differentiate after passage 5 (D) or 3 (E). Neural stem cell isolates from three to four animals per genotype were assessed. Data are displayed as mean ± SEM and were analyzed by two-way ANOVA (C) or unpaired, two-tailed Student's t test (E).

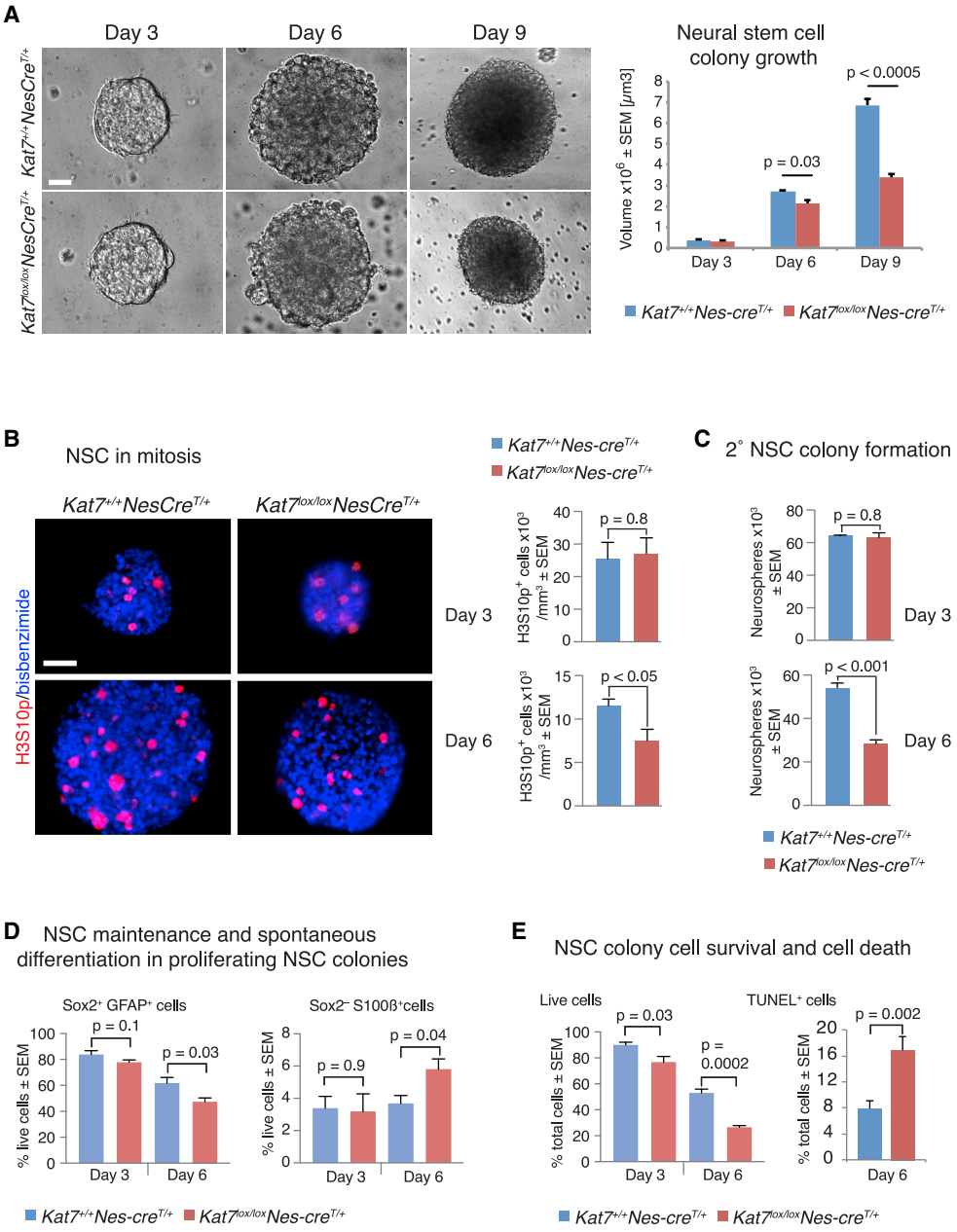

Figure 2. *Kat7*-deleted NSPCs have normal proliferative and self-renewal potential but increased cell death in culture

(A) Phase-contrast images and volume of *Kat7*$^{lox/lox}$*NesCre*$^{T/+}$ and *Kat7*$^{+/+}$*NesCre*$^{T/+}$ neurospheres on days 3, 6, and 9 after passage 5.

(B) Immunofluorescence staining and enumeration of mitotic cells marked by histone H3 phosphorylated on serine 10 (H3S10p) in *Kat7*$^{lox/lox}$*NesCre*$^{T/+}$ and *Kat7*$^{+/+}$*NesCre*$^{T/+}$ neurospheres on days 3 and 6 after passage 10. Passage 5 data are shown in Figure S5.

(C) Secondary neurosphere colony formation of *Kat7*$^{lox/lox}$*NesCre*$^{T/+}$ and *Kat7*$^{+/+}$*NesCre*$^{T/+}$ NSPCs on days 3 and 6 after passage 10. Passage 5 data are shown in Figure S5.

(D) Assessment of the percentage of SOX2^{+}GFAP^{+} neural stem cells and SOX2^{-}S100β^{+} astrocytes in proliferating *Kat7*$^{lox/lox}$*NesCre*$^{T/+}$ and *Kat7*$^{+/+}$*NesCre*$^{T/+}$ neurospheres. Flow cytometry gating strategy and median fluorescence intensities are shown in Figures S1 and S2.

(E) Percentage of live cells assessed by flow cytometry and TUNEL-positive cells after passage 5 in *Kat7*$^{lox/lox}$*NesCre*$^{T/+}$ and *Kat7*$^{+/+}$*NesCre*$^{T/+}$ neurospheres. Images of TUNEL staining are shown in Figure S5. Flow cytometry gating strategy is shown in Figure S1.

Neural stem cell isolates from three to four animals per genotype were assessed. Data are displayed as mean ± SEM and were analyzed by Student's t test. Scale bar indicates 18 μm in (A) (Day 3), 30 μm in (A) (Day 6), 60 μm in (A) (Day 9), and 43 μm in (C).

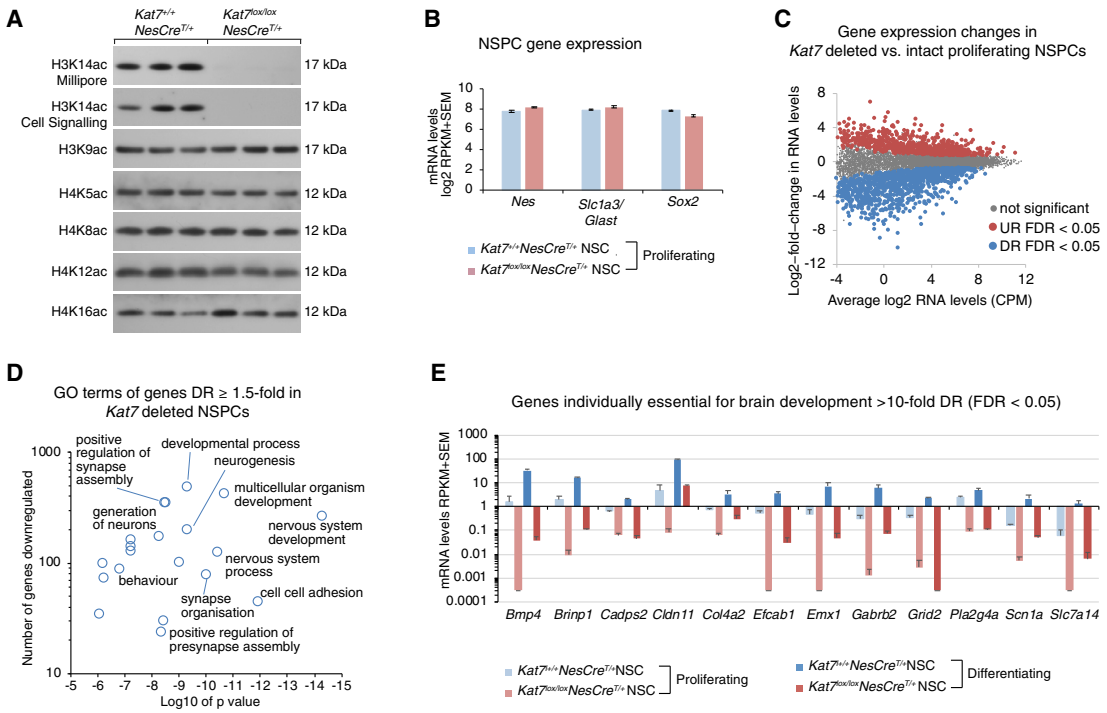

(legend on next page)

the first half of the passage interval and the second half of the passage interval suggests that the cell cycle could proceed in principle, but cell growth was affected by other factors (perhaps sensitivity to limiting nutrient and gas exchange in the later part of each passage interval), which may promote cell death and possibly astrocytic differentiation in *Kat7*$^{lox/lox}$*NesCre*$^{T/+}$ NSPCs.

Approximately 80% of proliferating NSPCs were GFAP/SOX2 double-positive congruent with previous observations suggesting that NSPCs are GFAP-positive, both *in vivo* and *in vitro*.[53–55]

Kat7-deleted NSPCs lose H3K14ac but express NSPC marker genes normally

Acetylation on histone H3 lysine 14 (H3K14ac) was lost in the *Kat7*$^{lox/lox}$*NesCre*$^{T/+}$ NSPCs compared with control cells, assessed using two different anti-H3K14ac antibodies (Figure 3A). In contrast, acetylation at five other histone H3 or H4 residues appeared unaffected (Figure 3A).

H3K14ac has previously been associated with actively expressed gene loci.[37,39,56] However, despite the profound loss of H3K14ac, *Kat7*$^{lox/lox}$*NesCre*$^{T/+}$ NSPCs expressed known NSPC marker genes, such as *Nes*, *Slc1a3*/*Glast,* and *Sox2* normally when compared with control NSPCs (Figure 3B, also see Figure 1B), as well as genes encoding the receptors of growth factors used in the neurosphere cultures (Figure S6).

Nevertheless, 1,778 protein-coding genes were at least 1.5-fold differentially expressed (DE) in proliferating NSPCs after loss of KAT7 (1,083 downregulated and 695 upregulated, false discovery rate [FDR] <0.05; Figure 3C and Table S1). Loss of KAT7 had no effects on the expression of other histone acetyltransferase genes (Figure S6).

Therefore, removal of KAT7 resulted in a loss of H3K14ac, but the mRNAs of genes typically expressed in NSPCs were maintained at normal levels.

Loss of KAT7 results in the repression of genes expressed at very low levels

Although known NSPC genes appeared unaffected by loss of KAT7, over 1,000 genes were downregulated in *Kat7*$^{lox/lox}$ *NesCre*$^{T/+}$ versus *Kat7*$^{+/+}$*NesCre*$^{T/+}$ proliferating NSPCs (Figures 3C and Table S1), but these appeared not to be essential for NSPC proliferation *in vitro* (see Figure 1C). Gene ontology (GO) term analysis revealed that genes ≥1.5-fold downregulated included genes required for nervous system and neuron development, synapse assembly, and regulation of behavior (Figures 3D and Table S2), which are processes not established in NSPCs prior to differentiation. In some cases, the downregulation of gene expression in proliferating NSPCs lacking KAT7 was dramatic (e.g., *Dcx* 68x, *Bdnf* 44x, *Clstn2* 23x, *Emx1* 15x; Table S1). A total of 304 protein-coding genes were substantially downregulated (≥10-fold; Table S1). Twelve of these genes were individually essential for brain development and function (Figure 3E). The ≥10-fold downregulated fraction further included genes mutated in neurological conditions, including seizures and autism-related disorders (Figure S6). In contrast, the substantially upregulated genes were mostly shared with other organ systems and involved in basic cellular functions (Figure S6 and Table S2).

Lack of KAT7 in differentiating NSPCs results in a failure to activate neuronal differentiation genes

The previous experiments suggested that KAT7 was particularly required for the expression of genes that are expressed at low levels in stem and progenitor cells. Among these were genes that are ordinarily upregulated during neuronal differentiation. To address the question if KAT7 was required for the upregulation of these genes during neuronal differentiation, we assessed the transcriptome of differentiating NSPCs compared with proliferating NSPCs (both *Kat7*$^{+/+}$*NesCre*$^{T/+}$ = *Kat7* intact) and

Figure 3. Loss of KAT7 results in loss of H3K14ac and repression of genes expressed at low levels

(A) Immunoblots of histone lysine acetylation levels at indicated residues in acid protein extracts of passage 5 *Kat7*$^{lox/lox}$*NesCre*$^{T/+}$ and *Kat7*$^{+/+}$*NesCre*$^{T/+}$ NSPCs. Each lane represents cells isolated from one animal, i.e., n = 3 animals per genotype. Two different antibodies were used to assess H3K14ac.

(B–I) RNA-seq data of NSPC isolates from four *Kat7*$^{lox/lox}$*NesCre*$^{T/+}$ and four *Kat7*$^{+/+}$*NesCre*$^{T/+}$ E14.5 fetuses for each, proliferating and differentiating conditions. NSPC isolates were kept in proliferating conditions for three passages and 3 days or differentiated for 3 days after passage 3. Data in (B) and (E) are displayed as mean ± SEM. Data were analyzed as stated under RNA-seq analysis. Differences with a transcriptome-wide FDR of <0.05 were considered significant.

Associated data are presented in Figure S6 and Tables S1, S2, S3, and S4, including RNA levels of all genes.

(B) Log_2 of reads per kilobase per million reads (RPKM) of NSPC marker genes *nestin*, *Slc1a3*/*Glast,* and *Sox2* in *Kat7*$^{lox/lox}$*NesCre*$^{T/+}$ and *Kat7*$^{+/+}$*NesCre*$^{T/+}$ NSPCs.

(C) Log_2 fold-change in RNA levels over log_2 of average RNA levels of in *Kat7*$^{lox/lox}$*NesCre*$^{T/+}$ and *Kat7*$^{+/+}$*NesCre*$^{T/+}$ NSPCs; upregulated genes (UR, red), downregulated genes (DR, blue), not significantly changed genes (gray).

(D) Gene ontology (GO) analysis of genes ≥1.5-fold downregulated (DR) in *Kat7*$^{lox/lox}$*NesCre*$^{T/+}$ versus *Kat7*$^{+/+}$*NesCre*$^{T/+}$ NSPCs, number of genes downregulated over log_{10} of p value.

(E) RPKM of genes ≥10-fold downregulated (DR) in *Kat7*$^{lox/lox}$*NesCre*$^{T/+}$ versus *Kat7*$^{+/+}$*NesCre*$^{T/+}$ NSPCs, which are individually essential for brain development and function.

(F) Heatmap of genes differentially expressed between *Kat7* intact proliferating versus differentiating NSPCs showing cell isolates from four *Kat7*$^{lox/lox}$*NesCre*$^{T/+}$ and four *Kat7*$^{+/+}$*NesCre*$^{T/+}$ E14.5 fetuses for the proliferating and differentiating condition. A group of genes, which are upregulated in *Kat7* intact differentiating versus proliferating NSPCs but fail to be upregulated in the *Kat7*$^{lox/lox}$*NesCre*$^{T/+}$ differentiating NSPCs, is marked in yellow at the left rim of the heatmap. These genes are further examined in (G), (H), and (I).

(G) Tissue expression annotation of genes that are upregulated in *Kat7* intact differentiating NSPCs but fail to be upregulated in the *Kat7*$^{lox/lox}$*NesCre*$^{T/+}$ differentiating NSPCs marked in yellow in (F).

(H) KEGG pathway analysis of genes that are upregulated in *Kat7* intact differentiating NSPCs but fail to be upregulated in the *Kat7*$^{lox/lox}$*NesCre*$^{T/+}$ differentiating NSPCs marked in yellow in (F).

(I) GO term annotation of genes that are upregulated in *Kat7* intact differentiating NSPCs but fail to be upregulated in the *Kat7*$^{lox/lox}$*NesCre*$^{T/+}$ differentiating NSPCs marked in yellow in (F).

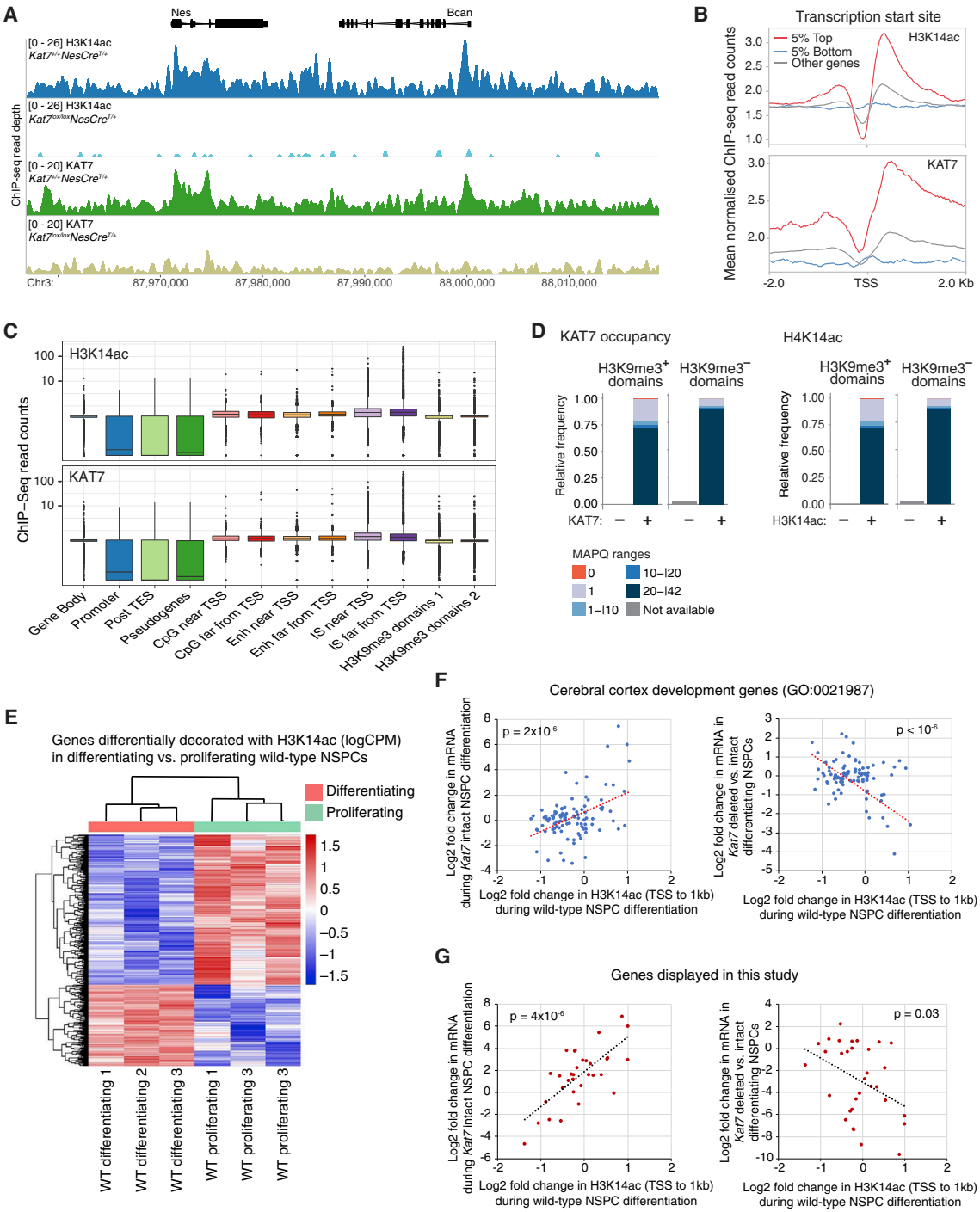

Figure 4. KAT7 and H3K14ac are widely distributed in the genome

(A–D) KAT7 genome occupancy and H3K14ac levels assessed by ChIP-seq at passage 5 day 3 of proliferating *Kat7*$^{lox/lox}$*NesCre*$^{T/+}$ and *Kat7*$^{+/+}$*NesCre*$^{T/+}$ NSPCs originally isolated at E14.5. NSPC isolates from three animals per genotype were assessed. Data were analyzed as stated under ChIP-seq analysis.

(A) Read depth plots of KAT7 occupancy (green, light green) and H3K14ac levels (blue, light blue) in *Kat7*$^{+/+}$*NesCre*$^{T/+}$ NSPCs and *Kat7*$^{lox/lox}$*NesCre*$^{T/+}$ NSPCs as indicated at the *Nes* and the *Bcan* locus. Note the paucity of H3K14ac ChIP-seq reads and reduction in KAT7 reads in the *Kat7*$^{lox/lox}$*NesCre*$^{T/+}$ NSPC (i.e., KAT7-deleted NSPCs, light blue, light green, respectively) allowing absolute rather than enrichment assessment. Further gene loci are shown in Figure S7.

(B) Mean normalized ChIP-seq read counts after alignment at transcription start sites (TSS) of genes segregated by expression level, after GC correction. DNA replication initiation sites, enhancers, and CpG islands are shown in Figure S8.

(C) Boxplots of KAT7 occupancy and H3K14ac levels as ChIP-seq read counts at various genomic features (first quartile, median, and third quartile of the distributions define the boxes). Significantly enriched are the counts in gene bodies, CpG islands, enhancers and DNA replication initiation sites (IS) compared

(legend continued on next page)

compared these to *Kat7*$^{lox/lox}$*NesCre*$^{T/+}$ NSPCs. We found a group of genes that is normally upregulated during NSPC differentiation but failed to be upregulated in differentiating *Kat7*$^{lox/lox}$*NesCre*$^{T/+}$ NSPCs (Figure 3F; marked in yellow; Tables S1 and S3). Tissue expression annotation identified these genes as nervous system expressed genes (Figure 3G and Table S4). Kyoto Encyclopedia of Genes and Genomes (KEGG) pathway and GO term analysis returned specific neuronal differentiation roles for these genes, including axon guidance, neuroactive ligand-receptor interaction, synapse functions, and cognition (Figures 3H and 3I, and Table S4).

SOX2 is a proposed pioneer transcription factor[8] and thought to initiate a neuronal program by activating genes including *Neurod1*.[9] *Sox2* mRNA was expressed (Figure 3B) and SOX2 protein was present in *Kat7*$^{lox/lox}$*NesCre*$^{T/+}$ NSPCs (Figure 1B), but SOX2 was unable to activate known target genes[9,57,58] adequately in differentiating *Kat7*$^{lox/lox}$*NesCre*$^{T/+}$ NSPCs (e.g., downregulated: *Neurod1* 3x, *Robo1* 5x, *Epha7* 7x, *Clstn2* 165x, *Stmn2* 249x; Table S3), suggesting that KAT7 and H3K14ac may be essential for the pioneer transcription factor function of SOX2.

KAT7 and H3K14ac occupy the genome broadly

Anti-KAT7 and anti-H3K14ac chromatin immunoprecipitation sequencing (ChIP-seq) experiments (Figures 4, S7, S8 and Table S5) of *Kat7*$^{lox/lox}$*NesCre*$^{T/+}$ versus *Kat7*$^{+/+}$*NesCre*$^{T/+}$ proliferating NSPCs allowed us to determine the absolute presence of H3K14ac and KAT7 occupancy in the genome, as well as areas of enrichment. We observed KAT7 and H3K14ac enrichment in specific neuronal and glial genes, such as *Nes*, *Bcan*, *Sox2*, *Olig1*, *Olig2*, *Spry2,* and *Spry4,* and a strong correlation between KAT7 occupancy and H3K14ac levels within genes (Figures 4A and S7). H3K14ac and KAT7 occupancy immediately downstream of the transcription start site (TSS) correlated positively with the level of gene expression (Figure 4B). Similarly, H3K14ac and KAT7 occupancy levels were positively correlated with expression levels of the nearest gene at enhancers and CpG islands (Figure S8). Importantly, we also observed KAT7 and H3K14ac reads clearly elevated above the *Kat7*$^{lox/lox}$*NesCre*$^{T/+}$ NSPCs (*Kat7* deleted) in all genes, including silent genes, and in intergenic regions throughout the genome. Genome-wide, H3K14ac and KAT7 occupancy was higher in gene bodies, CpG islands, enhancers, and DNA replication initiation sites (IS, as defined in Cayrou et al.[59]) than in pseudogenes, promoter regions, and 3′ of the transcription end site (TES; $p < 10^{-6}$ for all comparisons, Wilcoxon pairwise comparison, Figures 4B, 4C, and S8, and Table S5). Examination of domains that had previously been reported to be enriched for the heterochromatin mark H3K9 trimethylation (H3K9me3) in neural progenitor cells[60] revealed that KAT7 and H3K14ac were found in areas of the genome decorated by H3K9me3 (Figures 4C and Table S5). Levels of H3K14ac and KAT7 occupancy in H3K9me3 areas and the genome in general was not significantly affected by mappability of the reads (Figure 4D). Loss of KAT7 appeared to result in a decrease in H3K4me3 (at loci low for H3K27me3), but not RNA polymerase II (POLR2) occupancy (examined at example loci, Figure S8).

These data suggest that KAT7 and H3K14ac play a role not just at actively transcribed genes and DNA replication initiation sites, but are also present at repressed gene loci, in intergenic regions and heterochromatic regions.

Levels of H3K14ac correlate with mRNA levels during neuronal differentiation

Our NSPC differentiation, RNA expression, and H3K14ac data suggested that H3K14ac might be required for the activation of lineage-specific gene expression during neuronal differentiation. Therefore, we examined the relationship between mRNA levels and H3K14ac levels per gene in differentiating versus proliferating NSPCs. H3K14ac levels changed dramatically during wild-type NSPC differentiation (Figure 4E, Tables S6 and S7). The levels of H3K14ac (TSS to +1 kb) correlated positively with mRNA levels per gene in proliferating and differentiating wild-type NSPCs (both $p < 10^{-6}$; Figure S9). Importantly, the fold-change in H3K14ac levels upon differentiation correlated positively with the change in mRNA levels, generally for all genes ($p < 10^{-6}$; Figure S9) and specifically for cortex development genes ($p = 2 \times 10^{-6}$; Figure 4F), genes addressed in this study ($p = 4 \times 10^{-6}$; Figure 4G), and astrocyte differentiation genes ($p = 7 \times 10^{-5}$; Figure S9). In contrast, the difference in mRNA levels in *Kat7* deleted versus *Kat7* intact differentiating NSPCs correlated negatively with changes in H3K14ac levels in wild-type NSPCs upon differentiation, generally for all genes

with promoter regions, transcription end sites (TES), and pseudogenes (Bonferroni corrected $p < 10^{-16}$, Wilcoxon pairwise comparison, for all, but note multiplicity of tests, i.e., all genes in genome. Therefore, the focus is drawn here to the greatest differences).

(D) Presence of KAT7 and H3K14ac in H3K9me3 domains marking constitutive heterochromatin as assessed by frequency of 1-kb bins with KAT7 or H3K14ac that were positive or negative for H3K9me3 in neural progenitor cells (Bulut-Karslioglu et al.[60]; GSM1375164) stratified by mapping quality.

Further results are displayed in Figures S7 and S8 and Table S5, including correlation between KAT7 occupancy and H3K14ac levels, as well as H3K4me3, H3K27me3, and POLR2 ChIP-qPCR data.

(E–G) H3K14ac ChIP-seq data of NSPCs isolates from four wild-type (WT) E14.5 fetuses grown in proliferating and differentiating conditions. NSPC isolates were kept in proliferating conditions for three passages and 3 days or differentiated for 3 days after passage 3. Data were analyzed as stated under ChIP-seq analysis. ChIP-seq data were compared with RNA-seq data of *Kat7*$^{+/+}$*NesCre*$^{T/+}$ NSPCs and *Kat7*$^{lox/lox}$*NesCre*$^{T/+}$ NSPCs isolated from n = 4 E14.5 mouse fetuses per genotype. Associated data are presented in Figure S9 and Tables S6 and S7.

(E) Heatmap of protein-coding genes differentially decorated in the region TSS to +1 kb from the TSS comparing differentiating versus proliferating wild-type NSPCs.

(F) For cerebral cortex development genes (GO:0021987): correlation between the H3K14ac level fold-change (TSS to 1 kb; ChIP-seq) in wild-type NSPCs and mRNA levels (RNA-seq) of *Kat7*$^{+/+}$*NesCre*$^{T/+}$ NSPCs during differentiation (i.e., fold-change in differentiating versus proliferating); as well as correlation between the H3K14ac level fold-change (TSS to 1 kb; ChIP-seq) during differentiation of wild-type NSPCs and the fold-chance in mRNA levels between differentiating *Kat7*$^{+/+}$*NesCre*$^{T/+}$ NSPC and *Kat7*$^{lox/lox}$*NesCre*$^{T/+}$ NSPCs (RNA-seq). Protein-coding genes only.

(G) The same analysis as in (F), but for the genes displayed in this study.

($p < 10^{-6}$; Figure S9) and specifically for cortex development genes ($p < 10^{-6}$; Figure 4F) and gene addressed in this study ($p = 0.03$; Figure 4G), but not in astrocyte differentiation genes ($p = 0.2$; Figure S9). These results suggested that genes displaying an increase in H3K14ac during neuronal development were affected by loss of KAT7 and H3K14ac, but that astrocyte differentiation genes were less dependent on KAT7 and H3K14ac.

Loss of KAT7 in mid-neurogenesis results in abnormal cortex development and an increase in cell death

The preceding results suggested that KAT7 and H3K14ac have important functions in neural stem cell plasticity. To examine if KAT7 was required during cortex development, we deleted *Kat7* in early neurogenesis *in vivo*. While germline deletion of *Kat7* results in developmental arrest at E8.5,[33] the *NesCre* transgene deletes in the nervous system[61] and allowed *Kat7*$^{lox/lox}$*NesCre*$^{T/+}$ mice to develop to birth, but caused death at birth. In contrast, *Kat7*$^{+/-}$ heterozygous germline deleted[33] and *Kat7*$^{lox/+}$*NesCre*$^{T/+}$ heterozygously deleted mice were viable, healthy, and fertile. Homozygous loss of KAT7 in the nervous system caused a severe forebrain development defect (Figures 5 and S10). The depth of the E18.5 *Kat7*$^{lox/lox}$*NesCre*$^{T/+}$ cerebral cortex was reduced, cell density appeared increased, and the lateral ventricles were enlarged compared with *Kat7*$^{+/+}$*NesCre*$^{T/+}$ controls (Figures 5A and S10). The *Kat7*$^{lox/lox}$*NesCre*$^{T/+}$ corpus callosum, which consists of axon tracts connecting cortical neurons of both hemispheres, was reduced in diameter (Figure S10). The hippocampal formation was underdeveloped and the dentate gyrus rudimentary (Figure 5A). BrdU incorporation at E14.5, when rapid cell proliferation takes place in the developing cortex, was unaffected by *Kat7* deletion (Figures 5B and S10). In contrast, the *Kat7*$^{lox/lox}$*NesCre*$^{T/+}$ cortex displayed a more than 2-fold elevation in TUNEL^{+} cells compared with *Kat7*$^{+/+}$*NesCre*$^{T/+}$ controls (Figures 5B and S10).

The formation of cortical layers was disturbed in the *Kat7*$^{lox/lox}$*NesCre*$^{T/+}$ cortex, as assessed by layer marker expression (Figure 5C) and BrdU birth dating (not shown). The transcription factors SATB2, CTIP2, and TBR1 mark superficial, intermediate, and deep layers, respectively, of the developing cerebral cortex (Figure 5C). For assessment purposes, the cortex was divided into 10 pial to ventricle bins. In the *Kat7*$^{lox/lox}$*NesCre*$^{T/+}$ cortex, SATB2^{+} cells were underrepresented in the superficial layers (Figure 5C; $p = 0.03$, 0.007, and 0.045 for bins 2, 3, and 4). An abnormally high number of SATB2^{+}CTIP2^{+} double-positive cells (yellow) was observed in *Kat7*$^{lox/lox}$*NesCre*$^{T/+}$ superficial layers ($p = 0.007$, 0.02 for bins 1 and 2). CTIP2^{+} single positive cells were overrepresented in the *Kat7*$^{lox/lox}$*NesCre*$^{T/+}$ superficial layers ($p = 0.03$).

Cortical neurons (CNs) isolated from *Kat7*$^{lox/lox}$*NesCre*$^{T/+}$ E16.5 fetuses displayed a loss of KAT7 and H3K14ac compared with *Kat7*$^{+/+}$*NesCre*$^{T/+}$ control CN (Figure 5D). CNs of both genotypes appeared similar after overnight culture and had a similar proportion of cell death (Figures 5E and 5F). After 3 and 5 days of culture, *Kat7*$^{lox/lox}$*NesCre*$^{T/+}$ CNs displayed an increase in cell death compared with control cultures (Figure 5F), and live cells appeared progressively sparser (Figure S11).

GFAP^{+} astrocytes were observed in similar locations in the *Kat7*$^{lox/lox}$*NesCre*$^{T/+}$ as in the *Kat7*$^{+/+}$*NesCre*$^{T/+}$ control samples but appeared less abundant (Figure S12). S100β, marking maturing astrocytes, appeared less strongly expressed in the *Kat7*$^{lox/lox}$*NesCre*$^{T/+}$ compared with the *Kat7*$^{+/+}$*NesCre*$^{T/+}$ control samples.

These results show that cortex development was severely affected by the loss of KAT7, particularly affecting neurons born after the loss of KAT7 (upper layer neurons), but not affecting proliferation of ventricular zone progenitors. Astrocyte maturation may also be affected or delayed in the *Kat7*$^{lox/lox}$*NesCre*$^{T/+}$ cortex *in vivo*. The neuronal differentiation defect *in vivo* is similar to the phenotype observed in neural stem cells *in vitro*, albeit less strong, presumably due to persistence of some KAT7 protein and H3K14ac into the early phases of neurogenesis *in vivo* (time course of *Kat7* gene deletion and protein decline in Figure S10), whereas KAT7 and H3K14ac were completely absent before differentiation was induced in the cultured NSPCs (Figures 1A and 3A).

Loss of KAT7 in mid-neurogenesis causes failure of neuronal maturation gene expression

RNA sequencing (RNA-seq) of *Kat7*$^{lox/lox}$*NesCre*$^{T/+}$ and *Kat7*$^{+/+}$*NesCre*$^{T/+}$ E16.5 CNs cultured overnight (Figure 6 and Table S8) revealed that neuronal marker genes, including *Ncam1*, *Dcx*, *Bcl11b/Ctip2,* and *Neurod1,* were expressed at similar levels in both genotypes (Figure 6A). In contrast, mRNA levels of important cortex patterning genes, including *Pax6* and *Emx2*, were up to 3-fold reduced in the *Kat7*$^{lox/lox}$*NesCre*$^{T/+}$ CNs compared with controls (Figures 6A and Table S8). Discrepancies in genes affected by loss of KAT7 in CNs *ex vivo* compared with differentiating NSPCs *in vitro* may relate to the persistence of some KAT7 protein and H3K14ac into the early phases of neurogenesis *in vivo* (time course of *Kat7* gene deletion and protein decline in Figure S10), whereas KAT7 and H3K14ac were absent before differentiation was induced in the cultured NSPCs (Figures 1A and 3A).

Gene set analyses comparing the genes expressed in the *Kat7*$^{lox/lox}$*NesCre*$^{T/+}$ CNs with genes typical of embryonic stem cells, primitive ectoderm, transient neuroepithelial progenitors, neurogenic committed neuroepithelial progenitors, or neuronal rosettes (maturing neurons) showed that the gene expression profile in the KAT7 deficient cortical cells was most similar to transient, uncommitted neuroepithelial progenitors (Figure 6B). Congruent with this finding, KEGG pathway analysis revealed reduced expression of neuronal maturation genes in *Kat7*$^{lox/lox}$*NesCre*$^{T/+}$ CNs compared with controls, including neuroactive ligand-receptor interaction, synapse, and neurotransmitter signaling pathway genes (Figures 6C and Table S9). Unlike the downregulated genes, genes upregulated in *Kat7*$^{lox/lox}$*NesCre*$^{T/+}$ CNs compared with control cells did not show enriched pathways.

Timely re-expression of KAT7 restores neuronal and oligodendrocytic differentiation potential

Since neuronal and oligodendrocytic differentiation was particularly dependent on KAT7, we retrovirally expressed the full-length *Kat7* cDNA to determine if the effects of loss of KAT7 on NSPC differentiation were reversible. Overexpression of KAT7 in *Kat7*$^{lox/lox}$*NesCre*$^{T/+}$ 3 days after the initial loss of KAT7 (Figure 7A), resulted in partial restoration of H3K14ac in the *Kat7*$^{lox/lox}$*NesCre*$^{T/+}$ NSPCs, as compared with the empty vector control (Figure 7B)

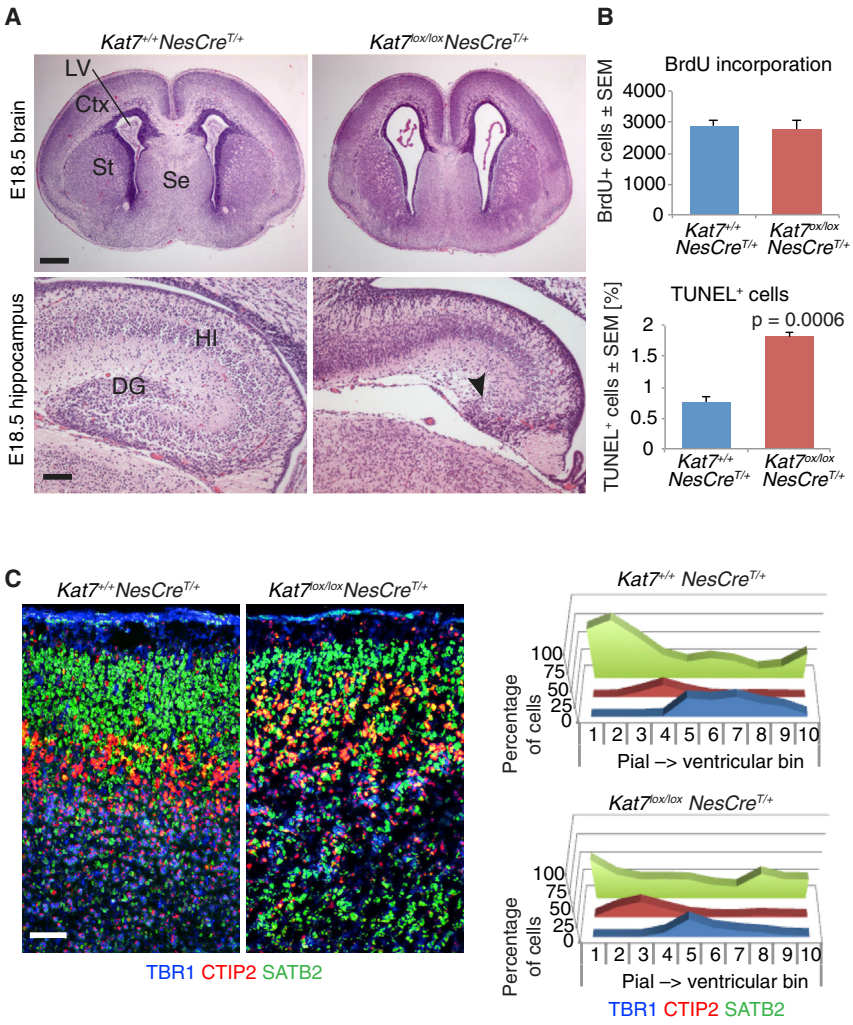

Figure 5. Loss of KAT7 causes brain developmental delay and increased cell death

(A) Hematoxylin and eosin-stained paraffin sections of E18.5 *Kat7*$^{lox/lox}$*NesCre*$^{T/+}$ and *Kat7*$^{+/+}$*NesCre*$^{T/+}$ forebrain at the level of the frontal cortex and the hippocampus. Arrowhead indicates rudimentary dentate gyrus (DG) cf. DG in control. Serial sections of the brains were examined. *Kat7* mRNA distribution by *in situ* hybridization, time courses of *Kat7* genetic deletion, decline in *Kat7* mRNA, and KAT7 protein levels are shown in Figure S10, as well as histone acetylation levels, gross brain morphology, and further histology.

(B) BrdU incorporation during DNA synthesis for 1 h and enumeration of cells undergoing TUNEL$^+$ cell death in E14.5 developing cerebral cortex. Images of BrdU and TUNEL staining are shown in Figure S10.

(C) Assessment of E18.5 cortical layer formation by immunofluorescence staining of markers for the deep layers (TBR1, blue), the intermediate layers (CTIP2, red), and the superficial layers (SATB2, green), and summary enumeration of cells in 10 pial to ventricular bins.

(D) Immunoblot assessment of KAT7 protein and H3K14ac levels in *Kat7*$^{lox/lox}$*NesCre*$^{T/+}$ and *Kat7*$^{+/+}$*NesCre*$^{T/+}$ E16.5 CNs cultured overnight. Each lane represents cells isolated from one animal, i.e., n = 3 mice per genotype. β-actin served as loading control.

(E) Phase-contrast images of *Kat7*$^{lox/lox}$*NesCre*$^{T/+}$ and *Kat7*$^{+/+}$*NesCre*$^{T/+}$ E16.5 cortical neurons (CNs) cultured overnight. A sequence of days 1–5 in culture is shown in Figure S11.

(F) Enumeration of cell death in *Kat7*$^{lox/lox}$*NesCre*$^{T/+}$ and *Kat7*$^{+/+}$*NesCre*$^{T/+}$ E16.5 CNs cultured for 1, 3, or 5 days.

Ctx, cerebral cortex; DG, dentate gyrus; Hi, hippocampus; LV, lateral ventricle; Se, septum, St, striatum. Scale bar, 800 μm in (A) (upper panels), 100 μm (lower panels), 50 μm in (C), and 105 μm in (E).

Three E18.5 brains per genotype were serially sectioned and stained. Data are displayed as mean ± SEM and were analyzed by Student's t test.

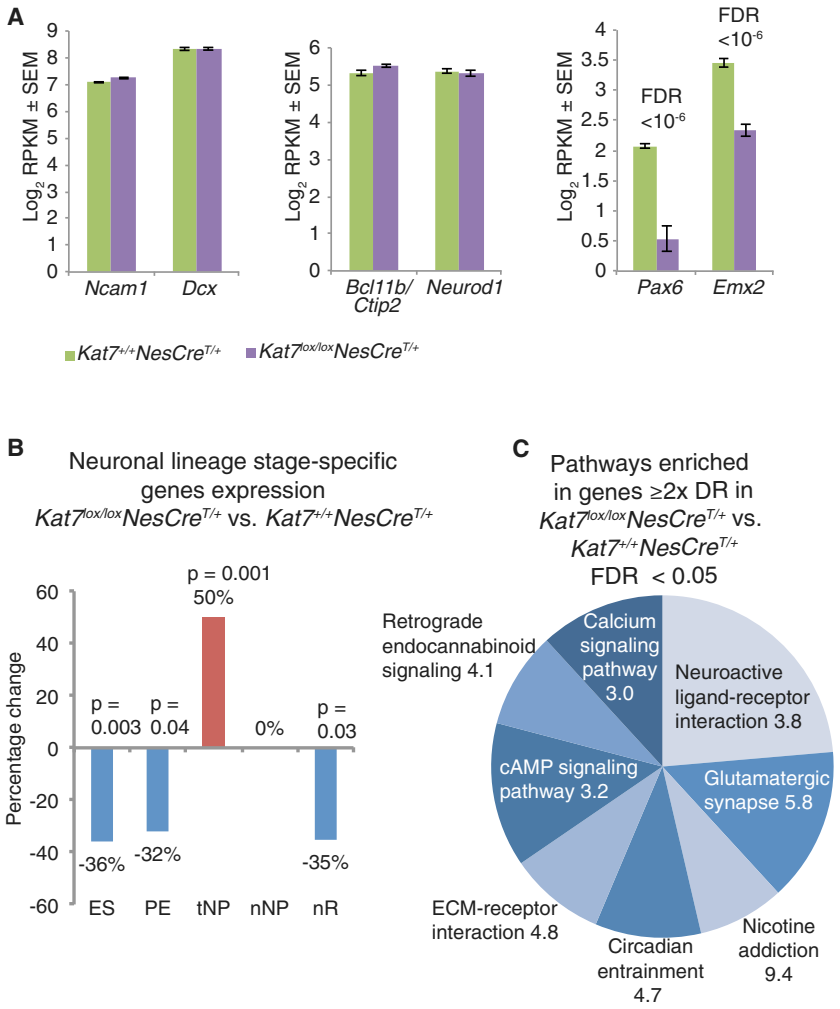

Figure 6. *Kat7* deletion during neurogenesis causes failure of neuronal maturation gene expression

(A–C) RNA-seq profiling of $Kat7^{lox/lox}NesCre^{T/+}$ and $Kat7^{+/+}NesCre^{T/+}$ E16.5 cortical neurons (CNs) cultured overnight. Further data in Tables S8 and S9.

(A) Log_2 of RPKM of neuronal marker genes and cerebral cortex patterning genes.

(B) ROAST enrichment analysis of gene sets representing embryonic stem cells (ES) differentiating toward the neuronal fate (neuronal rosettes, nR) with the intermediates primitive ectoderm (PE), transient neuronal progenitors (tNP), and committed neuronal progenitors (nNP) as defined in Abranches et al.[62] Enrichment (red) of genes designating transient neuronal progenitor stage (tNP) and depletion (blue) of genes designating the mature neuronal stage (nR) in $Kat7^{lox/lox}NesCre^{T/+}$ versus $Kat7^{+/+}NesCre^{T/+}$ E16.5 CN, while genes designating the committed neural progenitor stage (nNP) were neither enriched nor depleted. The figures show active proportions and one-side p values from ROAST.

(C) KEGG pathway analysis of genes ≥2-fold downregulated (DR) in $Kat7^{lox/lox}NesCre^{T/+}$ cf. $Kat7^{+/+}NesCre^{T/+}$ E16.5 CNs. The fold-enrichment of each pathway is indicated. Pathways with "Benjamini" adjusted p values <0.05 from DAVID are shown.

Cortical neuron isolates from four $Kat7^{lox/lox}NesCre^{T/+}$ and three $Kat7^{+/+}NesCre^{T/+}$ control animals were assessed. Data are displayed as mean ± SEM (A) and were analyzed as stated under RNA-seq analysis.

and restored neuronal and oligodendrocytic differentiation to normal (Figures 7C, 7D, and 7F).

Prolonged overexpression of KAT7 results in supernumerary neurons

Overexpression of KAT7 for 5 weeks in previously KAT7-deficient $Kat7^{lox/lox}NesCre^{T/+}$ NSPCs as well as in $Kat7^{+/+}NesCre^{T/+}$ control NSPCs resulted in substantially enhanced neuronal differentiation (Figures 7C and 7E). Oligodendrocytic differentiation was also substantially enhanced in $Kat7^{+/+}NesCre^{T/+}$ control NSPCs (Figure 7F). The observation that overexpression of KAT7 does not result in a significant increase in H3K14ac (Figure 7B) yet does result in a substantial increase in neurons (Figure 7C) and oligodendrocytes (Figure 7F) in $Kat7^{+/+}NesCre^{T/+}$ control NSPCs may reflect a change in H3K14ac levels in different parts of the genome or a possible ectopic function of overexpressed KAT7.

Brief window for quick restoration of neuronal differentiation potential

While re-expression of KAT7 after 3 days of absence resulted in a quick rescue of neuronal and oligodendrocytic differentiation potential (Figures 7A–7F), prolonged absence of KAT7 for 5 weeks resulted in resistance to restoration by short-term KAT7 re-expression (Figures 7G and 7H). However, prolonged re-expression of KAT7 for an additional 5 weeks resulted in some degree of rescue, even after the prolonged absence of KAT7 (Figures 7G and 7H).

These results show that neuronal and oligodendrocytic differentiation is dependent on KAT7 and can be enhanced by prolonged KAT7 overexpression.

DISCUSSION

Generating the loss of one specific histone modification for the purpose of studying its function is difficult in vertebrate organisms, because many modifications are catalyzed by two or more partially or fully redundant enzymes. Exceptionally, removal of KAT7 allowed us to investigate the role of KAT7 and H3K14ac in the regulation of gene expression in NSPCs and in the cortex during differentiation. The loss of H3K14ac in the absence of KAT7 and the high correlation between KAT7 genome occupancy and H3K14ac levels suggest that H3K14 is a major acetylation target of KAT7 in NSPCs.

While others reported that KAT7 catalyzes acetylation of histones H3 and H4 either in cell-free assays or detected as a global change by western blot in HEK293T cells,[28,29,37–39] we observed here, and others also found, that KAT7 predominantly acetylates histone H3K14 in mouse embryos and fibroblasts,[33] erythroblasts,[34] thymic epithelial cells,[36] and lung epithelial cells,[40] as

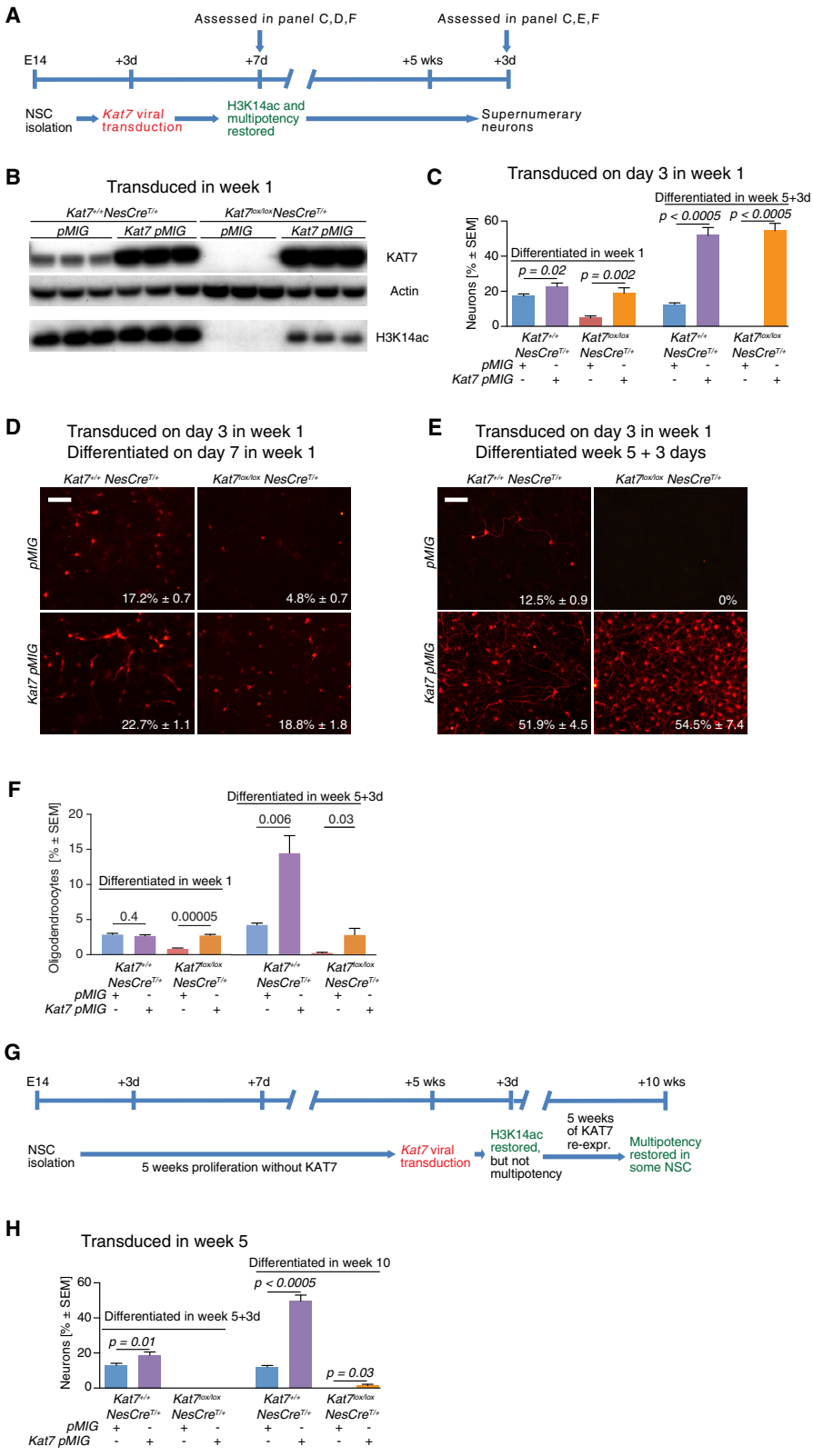

(legend on next page)

well as in human acute myeloid leukemia cells,[41] HeLa,[42–44] MCF7, and HEK293T cells.[44] A role of KAT7 in acetylating H4 could be concealed if other histone acetyltransferases compensated for the lack of KAT7 in H4 acetylation. Furthermore, H4 acetylation could be more prominent in cell types not examined here or locus-specific, not detectable by global assessment.

We showed that KAT7 and H3K14ac are distributed throughout the genome. The use of cells and tissues lacking KAT7 and H3K14ac allowed us to determine the "zero state" of H3K14ac in the genome and in so doing lend certainty to the H3K14ac ChIP signal above this "zero state." Previous reports were restricted to determining enrichment of H3K14ac over other areas of the genome, as is customary for ChIP-seq experiments, and observed KAT7 enrichment near TSS[37,39,56] and H3K14ac at gene loci and origins of DNA replication.[32,52] Consistent with previous reports,[32,37,39,52,56] we detected elevated levels of H3K14ac and KAT7 at highly expressed genes within the 5′ ~1 kb of the gene. Interestingly, H3K14ac and KAT7 did not appear to be essential for the continued expression of genes already active in NSPCs at the time of loss of KAT7, as these highly active genes continued to be expressed after *Kat7* deletion. In contrast, KAT7 appeared to be a prerequisite for very low levels of expression and, importantly, for activation to biologically relevant, cell fate-changing levels of transcription, which required KAT7 to be present continually prior to the activation event. An importance of maintaining the chromatin of gene loci open in stem cells for later activation during differentiation has been proposed previously[63] and is underscored by the observation that multipotency in stem cells requires a globally open chromatin state[64] associated with global gene expression.[65] Altogether, the broad distribution of H3K14ac in the genome observed here suggests a general role in genome organization maintaining the chromatin in an accessible conformation.

Previous work suggested that histone acetylation is largely restricted to transcriptionally active chromatin.[66] It was proposed that histone acetylation may not be required for initiation of transcription based on work in the fruit fly.[67] In contrast, we showed here that H3K14ac is present throughout the genome and that KAT7 is required for biologically relevant gene activation. In the absence of KAT7, gene activation is insufficient for cell fate changes. KAT7 is required for the activation of neuronal and oligodendrocytic differentiation genes (our study here). Previously, it had been reported that KAT7 was required for H3K14ac and the activation of early post-gastrulation embryonic patterning genes in the mouse,[33] and that H3K14ac was essential for larval wing disc differentiation gene expression and correct wing patterning in the fruit fly.[68] Taken together, these studies suggest that the main mechanism by which KAT7 ensures appropriate activation of patterning and differentiation genes is via H3K14ac.

The absence of H3K14ac and KAT7 resulted in a complete failure of neuronal and oligodendrocytic differentiation from NSPCs *in vitro*. In contrast, the loss of KAT7 during mid neurogenesis *in vivo* resulted in defective neuronal migration and maturation. The difference may be explained by the timing of KAT7 deletion. The NSPCs were isolated at E14.5, when KAT7 protein was already low, and were kept as proliferating cells for at least 3 weeks before differentiation was induced in the complete absence of KAT7. In contrast, while *Kat7* gene deletion and mRNA decline were complete *in vivo* at E12.5, when neurogenesis commences, KAT7 protein was still present at a quarter of the normal levels. This reduced level of KAT7 apparently was enough to allow the initial steps of neuronal differentiation but was not enough for migration and maturation. Alternatively, the more complex, supportive environment *in vivo* may have supported some level of neuronal differentiation in the absence of KAT7, but not migration and maturation. The failure of *Kat7* null NSPCs to give rise to neurons and oligodendrocytes, while successfully proliferating for at least 15 passages, suggests that *Kat7*-deleted NSPCs were capable of maintaining a status quo, but incapable of enacting a cell fate change in the absence of H3K14ac and KAT7. The failure of neuronal and oligodendrocytic differentiation, while astrocyte differentiation appeared to occur, suggests that KAT7 is essential for priming the gene network required for neural and oligodendrocyte differentiation pathways. In contrast, astrocyte differentiation may be a default pathway (in the absence of neural/oligo differentiation signals) and so unaffected, congruent with the observation that fetal and adult NSPCs share certain characteristics with astrocytes, such as GFAP expression.[53–55,69–72]

Kat7-deleted NSPCs failed to actively transcribe several transcription factor network modules known to be required for

Figure 7. Timely re-expression of KAT7 restores neuronal differentiation potential

(A) Timeline of the acute *Kat7* re-expression experiments. E14.5 NSPCs were cultured in NSPC proliferation medium for 3 days before viral transduction. *Kat7* or empty vector was overexpressed for 3 days or for 5 weeks before cells were differentiated.

(B) Immunoblot of KAT7 protein and H3K14ac in $Kat7^{lox/lox}NesCre^{T/+}$ and $Kat7^{+/+}NesCre^{T/+}$ NSPCs after retroviral expression of empty vector control (*pMIG*) or *Kat7* cDNA (*Kat7-pMIG*, *MSCV-Kat7-IRES-GFP*) in the first week after E14.5 NSPC isolation.

(C) Percentages of neurons formed during differentiation experiments, depicted in (D) and (E).

(D) Immunofluorescence staining for the neuronal marker type III β-tubulin (red) in differentiation cultures of $Kat7^{lox/lox}NesCre^{T/+}$ and $Kat7^{+/+}NesCre^{T/+}$ NSPCs 3 days after retroviral transduction with empty vector control (*pMIG*) or *Kat7* expression vector (*Kat7-pMIG*) in the first week after E14.5 NSPC isolation.

(E) As (D), except NSPCs overexpressing *Kat7* or empty vector were cultured for 5 weeks, before cells were differentiated.

(F) Percentages of oligodendrocytes formed during the differentiation experiments after acute, short, or long re-expression of *Kat7* as in (A).

(G) Timeline of the delayed *Kat7* re-expression experiments. NSPCs were cultured in NSPC proliferation medium for 5 weeks first before viral transduction. *Kat7* or empty vector was overexpressed from week 5 for 3 days or from week 5 to week 10, before cells were differentiated.

(H) Percentages of neurons formed after delayed re-expression of KAT7.

NSPC isolates from three to four animals per genotype were assessed in the different assay conditions in (A–H). Data are displayed as mean ± SEM and were analyzed by Student's t test. Scale bar, 80 μm.

Marker protein levels per cell are displayed in Figure S13.

neuronal differentiation. Interestingly, the pioneer transcription factor SOX2[8] was unable to activate target genes in the absence of KAT7. Timely re-expression of KAT7 restored NSPC plasticity completely, whereas delayed re-expression restored NSPC plasticity only partially and only after a prolonged period of re-expression for 5 weeks.

The ability of KAT7 overexpression to induce markedly enhanced neuronal differentiation may be of relevance to neuronal regeneration. NSPCs display a loss of neurogenic potential over passages in culture,[73,74] which limit their potential clinical use. Since overexpression of KAT7 resulted in the robust generation of supernumerary neurons, even after weeks in culture, it may be an avenue toward sustained neuron production.

Limitations of the study

Although our study provided clear results in the experimental paradigms tested, a number of limitations need to be taken into consideration. (1) While animal experiments provide data highly relevant to living organisms, the number of replicates that can be generated is limited to the minimum required by animal welfare considerations. (2) In our study, we used *C57BL/6* mice. *Kat7* deletion on another genetic background may produce different results. (3) The means of assessment of stem cell function for neural stem cells is not as comprehensive as for hematopoietic stem cells, where transplantation assays are readily used, e.g., Yang et al.[35] In particular, the precise functional relationship between the neurosphere formation assay *in vitro* and neural stem cell self-renewal *in vivo* remains unclear,[75] although *in vivo* and *in vitro* ablation studies have shown that the two functions correlate.[54,55] (4) Our study shows that H3K14ac is lost in the absence of KAT7, suggesting that KAT7 acetylates H3K14. However, the direct enzymatic action of KAT7 on H3K14 has not been demonstrated here. Indeed, in isolated cell-free experiments, histone acetyltransferases have been shown to promiscuously acetylate more histone lysine residues than are affected by their loss in cells (reviewed in Voss and Thomas[26]). Observations within cells return that loss of KAT7 specifically affects H3K14ac; however, other potential targets may be masked by compensatory actions within the more complex environment.

In conclusion, our data suggest that KAT7 is required to maintain H3K14ac genome-wide and that this is essential for developmental plasticity in NSPCs predominantly by promoting low-level expression of genes not essential in the stem cell state, but instead required for subsequent lineage differentiation.

STAR★METHODS

Detailed methods are provided in the online version of this paper and include the following:

- KEY RESOURCES TABLE
- RESOURCE AVAILABILITY
  - Lead contact
  - Materials availability
  - Data and code availability
- EXPERIMENTAL MODEL DETAILS
  - Mice
  - Cortical neurons isolation, culture and viability stain
  - NSPC isolation, culture and differentiation
- METHOD DETAILS
  - NSPC immunofluorescence
  - NSPC flow cytometry
  - Immunofluorescence for cortical layer formation
  - Immunofluorescence on E18 coronal brain sections
  - BrdU immunohistochemistry
  - TUNEL staining
  - Radioactive *in situ* hybridisation
  - Protein lysis, acid protein extraction and immunoblotting
  - Sample cohorts for RNA-seq and ChIP-seq experiments
  - RNA-seq profiling of cortical neurons
  - RNA-seq profiling of neural stem cells
  - ChIP-seq analysis
- QUANTIFICATION AND STATISTICAL ANALYSIS

SUPPLEMENTAL INFORMATION

Supplemental information can be found online at https://doi.org/10.1016/j.celrep.2022.111980.

ACKNOWLEDGMENTS

We gratefully acknowledge receipt of the *NesCre* transgenic mice, which G. Schütz kindly made available. We thank B. Ren and J. Stamatoyannopoulos for making available to the research community the ENCODE data GSE82598, GSE83172. We are grateful for excellent technical assistance received from F. Dabrowski, C. Gatt, T. McLennan, N. Senzo, E. Tsui, and T. Kawli. This work was funded by the Australian Government's National Health and Medical Research Council through Project Grants 1084352 (A.K.V., T.T.) and 1084248 (A.K.V., T.T.), a Program Grant 1054618 (T.P.S., G.K.S.), Research Fellowships (A.K.V. 575512 and 1081421; T.T. 1003435; T.P.S. 1082141; G.K.S. 1058892 and 1154970) and Investigator Grants (A.K.V. 1176789; B.P. 1175653), NIH grants HG00773509 and HG009442 to M.P.S. and the Independent Research Institutes Infrastructure Support (IRIIS) Scheme and a Victorian State Government OIS (Operational Infrastructure Support) Grant.

AUTHOR CONTRIBUTIONS

A.J.K. and M.B. conducted experiments, analyzed data, and drafted the manuscript. R.M., T.K., and S.W. conducted experiments. A.Q., B.P., C.L.W.S., I.L., Y.H., Z.P.F., C.W., and A.G. analyzed data. M.P.S., G.K.S., and T.P.S. supervised work and analyzed data. T.T. and A.K.V. conceived and supervised the project, analyzed data, and wrote the manuscript.

DECLARATION OF INTERESTS

The Thomas and Voss laboratories have received research funding from CTx CRC. M.P.S. is a cofounder and scientific advisor of Personalis, SensOmics, Qbio, January AI, Fodsel, Filtricine, Protos, RTHM, Iollo, Marble Therapeutics and Mirvie. He is a scientific advisor of Genapsys, Jupiter, Neuvivo, Swaza, Mitrix.

Received: February 25, 2019
Revised: September 30, 2022
Accepted: December 23, 2022

REFERENCES

1. Davis, A.A., and Temple, S. (1994). A self-renewing multipotential stem cell in embryonic rat cerebral cortex. Nature *372*, 263–266. https://doi.org/10.1038/372263a0.
2. Reynolds, B.A., and Weiss, S. (1992). Generation of neurons and astrocytes from isolated cells of the adult mammalian central nervous system. Science *255*, 1707–1710.
3. Beagan, J.A., Gilgenast, T.G., Kim, J., Plona, Z., Norton, H.K., Hu, G., Hsu, S.C., Shields, E.J., Lyu, X., Apostolou, E., et al. (2016). Local genome topology can exhibit an incompletely rewired 3D-folding state during somatic cell reprogramming. Cell Stem Cell *18*, 611–624. https://doi.org/10.1016/j.stem.2016.04.004.
4. Benayoun, B.A., Pollina, E.A., Ucar, D., Mahmoudi, S., Karra, K., Wong, E.D., Devarajan, K., Daugherty, A.C., Kundaje, A.B., Mancini, E., et al. (2014). H3K4me3 breadth is linked to cell identity and transcriptional consistency. Cell *158*, 673–688. https://doi.org/10.1016/j.cell.2014.06.027.
5. Kishi, Y., Fujii, Y., Hirabayashi, Y., and Gotoh, Y. (2012). HMGA regulates the global chromatin state and neurogenic potential in neocortical precursor cells. Nat. Neurosci. *15*, 1127–1133. https://doi.org/10.1038/nn.3165.
6. Paranjape, S.M., Kamakaka, R.T., and Kadonaga, J.T. (1994). Role of chromatin structure in the regulation of transcription by RNA polymerase II. Annu. Rev. Biochem. *63*, 265–297. https://doi.org/10.1146/annurev.bi.63.070194.001405.
7. Iwafuchi-Doi, M., and Zaret, K.S. (2016). Cell fate control by pioneer transcription factors. Development *143*, 1833–1837. https://doi.org/10.1242/dev.133900.
8. Liu, Z., and Kraus, W.L. (2017). Catalytic-independent functions of PARP-1 determine Sox2 pioneer activity at intractable genomic loci. Mol. Cell *65*, 589–603.e9. https://doi.org/10.1016/j.molcel.2017.01.017.
9. Amador-Arjona, A., Cimadamore, F., Huang, C.T., Wright, R., Lewis, S., Gage, F.H., and Terskikh, A.V. (2015). SOX2 primes the epigenetic landscape in neural precursors enabling proper gene activation during hippocampal neurogenesis. Proc. Natl. Acad. Sci. USA. *112*, E1936–E1945. https://doi.org/10.1073/pnas.1421480112.
10. Pataskar, A., Jung, J., Smialowski, P., Noack, F., Calegari, F., Straub, T., and Tiwari, V.K. (2016). NeuroD1 reprograms chromatin and transcription factor landscapes to induce the neuronal program. Embo j *35*, 24–45. https://doi.org/10.15252/embj.201591206.
11. Vierbuchen, T., Ostermeier, A., Pang, Z.P., Kokubu, Y., Südhof, T.C., and Wernig, M. (2010). Direct conversion of fibroblasts to functional neurons by defined factors. Nature *463*, 1035–1041. https://doi.org/10.1038/nature08797.
12. Agoston, Z., Heine, P., Brill, M.S., Grebbin, B.M., Hau, A.C., Kallenborn-Gerhardt, W., Schramm, J., Götz, M., and Schulte, D. (2014). Meis2 is a Pax6 co-factor in neurogenesis and dopaminergic periglomerular fate specification in the adult olfactory bulb. Development *141*, 28–38. https://doi.org/10.1242/dev.097295.
13. Mi, D., Carr, C.B., Georgala, P.A., Huang, Y.T., Manuel, M.N., Jeanes, E., Niisato, E., Sansom, S.N., Livesey, F.J., Theil, T., et al. (2013). Pax6 exerts regional control of cortical progenitor proliferation via direct repression of Cdk6 and hypophosphorylation of pRb. Neuron *78*, 269–284. https://doi.org/10.1016/j.neuron.2013.02.012.
14. Ninkovic, J., Steiner-Mezzadri, A., Jawerka, M., Akinci, U., Masserdotti, G., Petricca, S., Fischer, J., von Holst, A., Beckers, J., Lie, C.D., et al. (2013). The BAF complex interacts with Pax6 in adult neural progenitors to establish a neurogenic cross-regulatory transcriptional network. Cell Stem Cell *13*, 403–418. https://doi.org/10.1016/j.stem.2013.07.002.
15. Zhu, Q., Song, L., Peng, G., Sun, N., Chen, J., Zhang, T., Sheng, N., Tang, W., Qian, C., Qiao, Y., et al. (2014). The transcription factor Pou3f1 promotes neural fate commitment via activation of neural lineage genes and inhibition of external signaling pathways. Elife *3*, e02224. https://doi.org/10.7554/eLife.02224.
16. Yu, Y., Chen, Y., Kim, B., Wang, H., Zhao, C., He, X., Liu, L., Liu, W., Wu, L.M.N., Mao, M., et al. (2013). Olig2 targets chromatin remodelers to enhancers to initiate oligodendrocyte differentiation. Cell *152*, 248–261. https://doi.org/10.1016/j.cell.2012.12.006.
17. Zuchero, J.B., and Barres, B.A. (2013). Intrinsic and extrinsic control of oligodendrocyte development. Curr. Opin. Neurobiol. *23*, 914–920. https://doi.org/10.1016/j.conb.2013.06.005.
18. Wang, Z., Zang, C., Rosenfeld, J.A., Schones, D.E., Barski, A., Cuddapah, S., Cui, K., Roh, T.Y., Peng, W., Zhang, M.Q., and Zhao, K. (2008). Combinatorial patterns of histone acetylations and methylations in the human genome. Nat. Genet. *40*, 897–903. https://doi.org/10.1038/ng.154.
19. Wang, Z., Zang, C., Cui, K., Schones, D.E., Barski, A., Peng, W., and Zhao, K. (2009). Genome-wide mapping of HATs and HDACs reveals distinct functions in active and inactive genes. Cell *138*, 1019–1031. https://doi.org/10.1016/j.cell.2009.06.049.
20. Spitz, F., and Furlong, E.E.M. (2012). Transcription factors: from enhancer binding to developmental control. Nat. Rev. Genet. *13*, 613–626. https://doi.org/10.1038/nrg3207.
21. Bertero, A., Madrigal, P., Galli, A., Hubner, N.C., Moreno, I., Burks, D., Brown, S., Pedersen, R.A., Gaffney, D., Mendjan, S., et al. (2015). Activin/nodal signaling and NANOG orchestrate human embryonic stem cell fate decisions by controlling the H3K4me3 chromatin mark. Genes Dev. *29*, 702–717. https://doi.org/10.1101/gad.255984.114.
22. Lee, B., Lee, S., Agulnick, A.D., Lee, J.W., and Lee, S.K. (2016). Single-stranded DNA binding proteins are required for LIM complexes to induce transcriptionally active chromatin and specify spinal neuronal identities. Development *143*, 1721–1731. https://doi.org/10.1242/dev.131284.
23. Lee, K.K., and Workman, J.L. (2007). Histone acetyltransferase complexes: one size doesn't fit all. Nat. Rev. Mol. Cell Biol. *8*, 284–295. https://doi.org/10.1038/nrm2145.
24. Lee, D.Y., Hayes, J.J., Pruss, D., and Wolffe, A.P. (1993). A positive role for histone acetylation in transcription factor access to nucleosomal DNA. Cell *72*, 73–84.
25. Vettese-Dadey, M., Grant, P.A., Hebbes, T.R., Crane- Robinson, C., Allis, C.D., and Workman, J.L. (1996). Acetylation of histone H4 plays a primary role in enhancing transcription factor binding to nucleosomal DNA in vitro. Embo j *15*, 2508–2518.
26. Voss, A.K., and Thomas, T. (2018). Histone lysine and genomic targets of histone acetyltransferases in mammals. Bioessays *40*, e1800078. https://doi.org/10.1002/bies.201800078.
27. Burke, T.W., Cook, J.G., Asano, M., and Nevins, J.R. (2001). Replication factors MCM2 and ORC1 interact with the histone acetyltransferase HBO1. J. Biol. Chem. *276*, 15397–15408. https://doi.org/10.1074/jbc.M011556200.
28. Iizuka, M., and Stillman, B. (1999). Histone acetyltransferase HBO1 interacts with the ORC1 subunit of the human initiator protein. J. Biol. Chem. *274*, 23027–23034.
29. Doyon, Y., Cayrou, C., Ullah, M., Landry, A.J., Côté, V., Selleck, W., Lane, W.S., Tan, S., Yang, X.J., and Côté, J. (2006). ING tumor suppressor proteins are critical regulators of chromatin acetylation required for genome expression and perpetuation. Mol. Cell *21*, 51–64. https://doi.org/10.1016/j.molcel.2005.12.007.
30. Miotto, B., and Struhl, K. (2008). HBO1 histone acetylase is a coactivator of the replication licensing factor Cdt1. Genes Dev. *22*, 2633–2638. https://doi.org/10.1101/gad.1674108.
31. Miotto, B., and Struhl, K. (2010). HBO1 histone acetylase activity is essential for DNA replication licensing and inhibited by Geminin. Mol. Cell *37*, 57–66. https://doi.org/10.1016/j.molcel.2009.12.012.
32. Feng, Y., Vlassis, A., Roques, C., Lalonde, M.E., González-Aguilera, C., Lambert, J.P., Lee, S.B., Zhao, X., Alabert, C., Johansen, J.V., et al. (2016). BRPF3-HBO1 regulates replication origin activation and histone H3K14 acetylation. Embo j *35*, 176–192. https://doi.org/10.15252/embj.201591293.

33. Kueh, A.J., Dixon, M.P., Voss, A.K., and Thomas, T. (2011). HBO1 is required for H3K14 acetylation and normal transcriptional activity during embryonic development. Mol. Cell Biol. *31*, 845–860. https://doi.org/10.1128/MCB.00159-10.

34. Mishima, Y., Miyagi, S., Saraya, A., Negishi, M., Endoh, M., Endo, T.A., Toyoda, T., Shinga, J., Katsumoto, T., Chiba, T., et al. (2011). The Hbo1-Brd1/Brpf2 complex is responsible for global acetylation of H3K14 and required for fetal liver erythropoiesis. Blood *118*, 2443–2453. https://doi.org/10.1182/blood-2011-01-331892.

35. Yang, Y., Kueh, A.J., Grant, Z.L., Abeysekera, W., Garnham, A.L., Wilcox, S., Hyland, C.D., Di Rago, L., Metcalf, D., Alexander, W.S., et al. (2022). The histone lysine acetyltransferase HBO1 (KAT7) regulates hematopoietic stem cell quiescence and self-renewal. Blood *139*, 845–858. https://doi.org/10.1182/blood.2021013954.

36. Heinlein, M., Gandolfo, L.C., Zhao, K., Teh, C.E., Nguyen, N., Baell, J.B., Goldfarb, Y., Abramson, J., Wichmann, J., Voss, A.K., et al. (2022). The acetyltransferase KAT7 is required for thymic epithelial cell expansion, expression of AIRE target genes, and thymic tolerance. Sci. Immunol. *7*, eabb6032. https://doi.org/10.1126/sciimmunol.abb6032.

37. Lalonde, M.E., Avvakumov, N., Glass, K.C., Joncas, F.H., Saksouk, N., Holliday, M., Paquet, E., Yan, K., Tong, Q., Klein, B.J., et al. (2013). Exchange of associated factors directs a switch in HBO1 acetyltransferase histone tail specificity. Genes Dev. *27*, 2009–2024. https://doi.org/10.1101/gad.223396.113.

38. Niida, H., Matsunuma, R., Horiguchi, R., Uchida, C., Nakazawa, Y., Motegi, A., Nishimoto, K., Sakai, S., Ohhata, T., Kitagawa, K., et al. (2017). Phosphorylated HBO1 at UV irradiated sites is essential for nucleotide excision repair. Nat. Commun. *8*, 16102. https://doi.org/10.1038/ncomms16102.

39. Saksouk, N., Avvakumov, N., Champagne, K.S., Hung, T., Doyon, Y., Cayrou, C., Paquet, E., Ullah, M., Landry, A.J., Côté, V., et al. (2009). HBO1 HAT complexes target chromatin throughout gene coding regions via multiple PHD finger interactions with histone H3 tail. Mol. Cell *33*, 257–265. https://doi.org/10.1016/j.molcel.2009.01.007.

40. Zou, C., Chen, Y., Smith, R.M., Snavely, C., Li, J., Coon, T.A., Chen, B.B., Zhao, Y., and Mallampalli, R.K. (2013). SCF Fbxw15 mediates histone acetyltransferase binding to origin recognition complex (HBO1) ubiquitin-proteasomal degradation to regulate cell proliferation. J. Biol. Chem. *288*, 6306–6316. https://doi.org/10.1074/jbc.M112.426882.

41. MacPherson, L., Anokye, J., Yeung, M.M., Lam, E.Y.N., Chan, Y.C., Weng, C.F., Yeh, P., Knezevic, K., Butler, M.S., Hoegl, A., et al. (2020). HBO1 is required for the maintenance of leukaemia stem cells. Nature *577*, 266–270. https://doi.org/10.1038/s41586-019-1835-6.

42. Matsunuma, R., Niida, H., Ohhata, T., Kitagawa, K., Sakai, S., Uchida, C., Shiotani, B., Matsumoto, M., Nakayama, K.I., Ogura, H., et al. (2016). UV damage-induced phosphorylation of HBO1 triggers CRL4DDB2-mediated degradation to regulate cell proliferation. Mol. Cell Biol. *36*, 394–406. https://doi.org/10.1128/mcb.00809-15.

43. Ohzeki, J.I., Shono, N., Otake, K., Martins, N.M.C., Kugou, K., Kimura, H., Nagase, T., Larionov, V., Earnshaw, W.C., and Masumoto, H. (2016). KAT7/HBO1/MYST2 regulates CENP-A chromatin assembly by antagonizing Suv39h1-mediated centromere inactivation. Dev. Cell *37*, 413–427. https://doi.org/10.1016/j.devcel.2016.05.006.

44. Kueh, A.J., Eccles, S., Tang, L., Garnham, A.L., May, R.E., Herold, M.J., Smyth, G.K., Voss, A.K., and Thomas, T. (2020). HBO1 (KAT7) does not have an essential role in cell proliferation, DNA replication, or histone 4 acetylation in human cells. Mol. Cell Biol. *40*, e00506–e00519. https://doi.org/10.1128/mcb.00506-19.

45. Grant, Z.L., Hickey, P.F., Abeysekera, W., Whitehead, L., Lewis, S.M., Symons, R.C.A., Baldwin, T.M., Amann-Zalcenstein, D., Garnham, A.L., Naik, S.H., et al. (2021). The histone acetyltransferase HBO1 promotes efficient tip cell sprouting during angiogenesis. Development *148*, dev199581. https://doi.org/10.1242/dev.199581.

46. Newman, D.M., Voss, A.K., Thomas, T., and Allan, R.S. (2017). Essential role for the histone acetyltransferase KAT7 in T cell development, fitness, and survival. J. Leukoc. Biol. *101*, 887–892. https://doi.org/10.1189/jlb.1MA0816-338R.

47. Kuo, M.H., Brownell, J.E., Sobel, R.E., Ranalli, T.A., Cook, R.G., Edmondson, D.G., Roth, S.Y., and Allis, C.D. (1996). Transcription-linked acetylation by Gcn5p of histones H3 and H4 at specific lysines. Nature *383*, 269–272. https://doi.org/10.1038/383269a0.

48. Lo, W.S., Trievel, R.C., Rojas, J.R., Duggan, L., Hsu, J.Y., Allis, C.D., Marmorstein, R., and Berger, S.L. (2000). Phosphorylation of serine 10 in histone H3 is functionally linked in vitro and in vivo to Gcn5-mediated acetylation at lysine 14. Mol. Cell *5*, 917–926.

49. Pokholok, D.K., Harbison, C.T., Levine, S., Cole, M., Hannett, N.M., Lee, T.I., Bell, G.W., Walker, K., Rolfe, P.A., Herbolsheimer, E., et al. (2005). Genome-wide map of nucleosome acetylation and methylation in yeast. Cell *122*, 517–527. https://doi.org/10.1016/j.cell.2005.06.026.

50. Johnsson, A., Durand-Dubief, M., Xue-Franzén, Y., Rönnerblad, M., Ekwall, K., and Wright, A. (2009). HAT-HDAC interplay modulates global histone H3K14 acetylation in gene-coding regions during stress. EMBO Rep. *10*, 1009–1014.

51. Luebben, W.R., Sharma, N., and Nyborg, J.K. (2010). Nucleosome eviction and activated transcription require p300 acetylation of histone H3 lysine 14. Proc. Natl. Acad. Sci. USA. *107*, 19254–19259. https://doi.org/10.1073/pnas.1009650107.

52. Karmodiya, K., Krebs, A.R., Oulad-Abdelghani, M., Kimura, H., and Tora, L. (2012). H3K9 and H3K14 acetylation co-occur at many gene regulatory elements, while H3K14ac marks a subset of inactive inducible promoters in mouse embryonic stem cells. BMC Genom. *13*, 424. https://doi.org/10.1186/1471-2164-13-424.

53. Götz, M., Sirko, S., Beckers, J., and Irmler, M. (2015). Reactive astrocytes as neural stem or progenitor cells: in vivo lineage, in vitro potential, and Genome-wide expression analysis. Glia *63*, 1452–1468. https://doi.org/10.1002/glia.22850.

54. Imura, T., Kornblum, H.I., and Sofroniew, M.V. (2003). The predominant neural stem cell isolated from postnatal and adult forebrain but not early embryonic forebrain expresses GFAP. J. Neurosci. *23*, 2824–2832. https://doi.org/10.1523/jneurosci.23-07-02824.2003.

55. Morshead, C.M., Garcia, A.D., Sofroniew, M.V., and van Der Kooy, D. (2003). The ablation of glial fibrillary acidic protein-positive cells from the adult central nervous system results in the loss of forebrain neural stem cells but not retinal stem cells. Eur. J. Neurosci. *18*, 76–84. https://doi.org/10.1046/j.1460-9568.2003.02727.x.

56. Avvakumov, N., Lalonde, M.E., Saksouk, N., Paquet, E., Glass, K.C., Landry, A.J., Doyon, Y., Cayrou, C., Robitaille, G.A., Richard, D.E., et al. (2012). Conserved molecular interactions within the HBO1 acetyltransferase complexes regulate cell proliferation. Mol. Cell Biol. *32*, 689–703. https://doi.org/10.1128/MCB.06455-11.

57. Boumahdi, S., Driessens, G., Lapouge, G., Rorive, S., Nassar, D., Le Mercier, M., Delatte, B., Caauwe, A., Lenglez, S., Nkusi, E., et al. (2014). SOX2 controls tumour initiation and cancer stem-cell functions in squamous-cell carcinoma. Nature *511*, 246–250. https://doi.org/10.1038/nature13305.

58. Dun, X.P., Carr, L., Woodley, P.K., Barry, R.W., Drake, L.K., Mindos, T., Roberts, S.L., Lloyd, A.C., and Parkinson, D.B. (2019). Macrophage-Derived Slit3 controls cell migration and axon pathfinding in the peripheral nerve bridge. Cell Rep. *26*, 1458–1472.e4. https://doi.org/10.1016/j.celrep.2018.12.081.

59. Cayrou, C., Ballester, B., Peiffer, I., Fenouil, R., Coulombe, P., Andrau, J.C., van Helden, J., and Méchali, M. (2015). The chromatin environment shapes DNA replication origin organization and defines origin classes. Genome Res. *25*, 1873–1885. https://doi.org/10.1101/gr.192799.115.

60. Bulut-Karslioglu, A., De La Rosa-Velázquez, I.A., Ramirez, F., Barenboim, M., Onishi-Seebacher, M., Arand, J., Galán, C., Winter, G.E., Engist, B., Gerle, B., et al. (2014). Suv39h-dependent H3K9me3 marks intact

retrotransposons and silences LINE elements in mouse embryonic stem cells. Mol. Cell *55*, 277–290. https://doi.org/10.1016/j.molcel.2014.05.029.

61. Tronche, F., Kellendonk, C., Kretz, O., Gass, P., Anlag, K., Orban, P.C., Bock, R., Klein, R., and Schütz, G. (1999). Disruption of the glucocorticoid receptor gene in the nervous system results in reduced anxiety. Nat. Genet. *23*, 99–103. https://doi.org/10.1038/12703.

62. Abranches, E., Silva, M., Pradier, L., Schulz, H., Hummel, O., Henrique, D., and Bekman, E. (2009). Neural differentiation of embryonic stem cells in vitro: a road map to neurogenesis in the embryo. PLoS One *4*, e6286. https://doi.org/10.1371/journal.pone.0006286.

63. Efroni, S., Melcer, S., Nissim-Rafinia, M., and Meshorer, E. (2009). Stem cells do play with dice: a statistical physics view of transcription. Cell Cycle *8*, 43–48. https://doi.org/10.4161/cc.8.1.7216.

64. Gaspar-Maia, A., Alajem, A., Polesso, F., Sridharan, R., Mason, M.J., Heidersbach, A., Ramalho-Santos, J., McManus, M.T., Plath, K., Meshorer, E., and Ramalho-Santos, M. (2009). Chd1 regulates open chromatin and pluripotency of embryonic stem cells. Nature *460*, 863–868. https://doi.org/10.1038/nature08212.

65. Efroni, S., Duttagupta, R., Cheng, J., Dehghani, H., Hoeppner, D.J., Dash, C., Bazett-Jones, D.P., Le Grice, S., McKay, R.D.G., Buetow, K.H., et al. (2008). Global transcription in pluripotent embryonic stem cells. Cell Stem Cell *2*, 437–447. https://doi.org/10.1016/j.stem.2008.03.021.

66. Lawrence, M., Daujat, S., and Schneider, R. (2016). Lateral thinking: how histone modifications regulate gene expression. Trends Genet. *32*, 42–56. https://doi.org/10.1016/j.tig.2015.10.007.

67. Pérez-Lluch, S., Blanco, E., Tilgner, H., Curado, J., Ruiz-Romero, M., Corominas, M., and Guigó, R. (2015). Absence of canonical marks of active chromatin in developmentally regulated genes. Nat. Genet. *47*, 1158–1167. https://doi.org/10.1038/ng.3381.

68. Regadas, I., Dahlberg, O., Vaid, R., Ho, O., Belikov, S., Dixit, G., Deindl, S., Wen, J., and Mannervik, M. (2021). A unique histone 3 lysine 14 chromatin signature underlies tissue-specific gene regulation. Mol. Cell *81*, 1766–1780.e10. https://doi.org/10.1016/j.molcel.2021.01.041.

69. Hartfuss, E., Galli, R., Heins, N., and Götz, M. (2001). Characterization of CNS precursor subtypes and radial glia. Dev. Biol. *229*, 15–30. https://doi.org/10.1006/dbio.2000.9962.

70. Heins, N., Malatesta, P., Cecconi, F., Nakafuku, M., Tucker, K.L., Hack, M.A., Chapouton, P., Barde, Y.A., and Götz, M. (2002). Glial cells generate neurons: the role of the transcription factor Pax6. Nat. Neurosci. *5*, 308–315. https://doi.org/10.1038/nn828.

71. Noctor, S.C., Flint, A.C., Weissman, T.A., Dammerman, R.S., and Kriegstein, A.R. (2001). Neurons derived from radial glial cells establish radial units in neocortex. Nature *409*, 714–720. https://doi.org/10.1038/35055553.

72. Noctor, S.C., Flint, A.C., Weissman, T.A., Wong, W.S., Clinton, B.K., and Kriegstein, A.R. (2002). Dividing precursor cells of the embryonic cortical ventricular zone have morphological and molecular characteristics of radial glia. J. Neurosci. *22*, 3161–3173. https://doi.org/10.1523/jneurosci.22-08-03161.2002.

73. Fasano, C.A., Phoenix, T.N., Kokovay, E., Lowry, N., Elkabetz, Y., Dimos, J.T., Lemischka, I.R., Studer, L., and Temple, S. (2009). Bmi-1 cooperates with Foxg1 to maintain neural stem cell self-renewal in the forebrain. Genes Dev. *23*, 561–574. https://doi.org/10.1101/gad.1743709.

74. Groszer, M., Erickson, R., Scripture-Adams, D.D., Dougherty, J.D., Le Belle, J., Zack, J.A., Geschwind, D.H., Liu, X., Kornblum, H.I., and Wu, H. (2006). PTEN negatively regulates neural stem cell self-renewal by modulating G0-G1 cell cycle entry. Proc. Natl. Acad. Sci. USA. *103*, 111–116. https://doi.org/10.1073/pnas.0509939103.

75. Pastrana, E., Silva-Vargas, V., and Doetsch, F. (2011). Eyes wide open: a critical review of sphere-formation as an assay for stem cells. Cell Stem Cell *8*, 486–498. https://doi.org/10.1016/j.stem.2011.04.007.

76. Voss, A.K., Britto, J.M., Dixon, M.P., Sheikh, B.N., Collin, C., Tan, S.S., and Thomas, T. (2008). C3G regulates cortical neuron migration, preplate splitting and radial glial cell attachment. Development *135*, 2139–2149. https://doi.org/10.1242/dev.016725.

77. Merson, T.D., Dixon, M.P., Collin, C., Rietze, R.L., Bartlett, P.F., Thomas, T., and Voss, A.K. (2006). The transcriptional coactivator Querkopf controls adult neurogenesis. J. Neurosci. *26*, 11359–11370.

78. Thomas, T., Voss, A.K., Chowdhury, K., and Gruss, P. (2000). Querkopf, a MYST family histone acetyltransferase, is required for normal cerebral cortex development. Development *127*, 2537–2548.

79. Liao, Y., Smyth, G.K., and Shi, W. (2013). The Subread aligner: fast, accurate and scalable read mapping by seed-and-vote. Nucleic Acids Res. *41*, e108. https://doi.org/10.1093/nar/gkt214.

80. Liao, Y., Smyth, G.K., and Shi, W. (2014). featureCounts: an efficient general purpose program for assigning sequence reads to genomic features. Bioinformatics *30*, 923–930. https://doi.org/10.1093/bioinformatics/btt656.

81. Robinson, M.D., and Oshlack, A. (2010). A scaling normalization method for differential expression analysis of RNA-seq data. Genome Biol. *11*, R25. https://doi.org/10.1186/gb-2010-11-3-r25.

82. Robinson, M.D., and Smyth, G.K. (2008). Small-sample estimation of negative binomial dispersion, with applications to SAGE data. Biostatistics *9*, 321–332. https://doi.org/10.1093/biostatistics/kxm030.

83. Robinson, M.D., McCarthy, D.J., and Smyth, G.K. (2010). edgeR: a Bioconductor package for differential expression analysis of digital gene expression data. Bioinformatics *26*, 139–140. https://doi.org/10.1093/bioinformatics/btp616.

84. Law, C.W., Chen, Y., Shi, W., and Smyth, G.K. (2014). voom: precision weights unlock linear model analysis tools for RNA-seq read counts. Genome Biol. *15*, R29. https://doi.org/10.1186/gb-2014-15-2-r29.

85. Wu, D., Lim, E., Vaillant, F., Asselin-Labat, M.L., Visvader, J.E., and Smyth, G.K. (2010). ROAST: rotation gene set tests for complex microarray experiments. Bioinformatics *26*, 2176–2182. https://doi.org/10.1093/bioinformatics/btq401.

86. Abrajano, J.J., Qureshi, I.A., Gokhan, S., Zheng, D., Bergman, A., and Mehler, M.F. (2009). Differential deployment of REST and CoREST promotes glial subtype specification and oligodendrocyte lineage maturation. PLoS One *4*, e7665. https://doi.org/10.1371/journal.pone.0007665.

87. Geatrell, J.C., Gan, P.M.I., Mansergh, F.C., Kisiswa, L., Jarrin, M., Williams, L.A., Evans, M.J., Boulton, M.E., and Wride, M.A. (2009). Apoptosis gene profiling reveals spatio-temporal regulated expression of the p53/Mdm2 pathway during lens development. Exp. Eye Res. *88*, 1137–1151. https://doi.org/10.1016/j.exer.2009.01.020.

88. Lee, G., Kim, H., Elkabetz, Y., Al Shamy, G., Panagiotakos, G., Barberi, T., Tabar, V., and Studer, L. (2007). Isolation and directed differentiation of neural crest stem cells derived from human embryonic stem cells. Nat. Biotechnol. *25*, 1468–1475. https://doi.org/10.1038/nbt1365.

89. Subramanian, A., Tamayo, P., Mootha, V.K., Mukherjee, S., Ebert, B.L., Gillette, M.A., Paulovich, A., Pomeroy, S.L., Golub, T.R., Lander, E.S., and Mesirov, J.P. (2005). Gene set enrichment analysis: a knowledge-based approach for interpreting genome-wide expression profiles. Proc. Natl. Acad. Sci. USA. *102*, 15545–15550. https://doi.org/10.1073/pnas.0506580102.

90. Huang, D.W., Sherman, B.T., and Lempicki, R.A. (2009). Systematic and integrative analysis of large gene lists using DAVID bioinformatics resources. Nat. Protoc. *4*, 44–57. https://doi.org/10.1038/nprot.2008.211.

91. Huang, D.W., Sherman, B.T., and Lempicki, R.A. (2009). Bioinformatics enrichment tools: paths toward the comprehensive functional analysis of large gene lists. Nucleic Acids Res. *37*, 1–13. https://doi.org/10.1093/nar/gkn923.

92. Liao, Y., Smyth, G.K., and Shi, W. (2019). The R package Rsubread is easier, faster, cheaper and better for alignment and quantification of

RNA sequencing reads. Nucleic Acids Res. *47*, e47. https://doi.org/10.1093/nar/gkz114.

93. Ritchie, M.E., Phipson, B., Wu, D., Hu, Y., Law, C.W., Shi, W., and Smyth, G.K. (2015). Limma powers differential expression analyses for RNA-sequencing and microarray studies. Nucleic Acids Res. *43*, e47. https://doi.org/10.1093/nar/gkv007.

94. Liu, R., Holik, A.Z., Su, S., Jansz, N., Chen, K., Leong, H.S., Blewitt, M.E., Asselin-Labat, M.L., Smyth, G.K., and Ritchie, M.E. (2015). Why weight? Modelling sample and observational level variability improves power in RNA-seq analyses. Nucleic Acids Res. *43*, e97. https://doi.org/10.1093/nar/gkv412.

95. McCarthy, D.J., and Smyth, G.K. (2009). Testing significance relative to a fold-change threshold is a TREAT. Bioinformatics *25*, 765–771. https://doi.org/10.1093/bioinformatics/btp053.

96. Voss, A.K., Dixon, M.P., McLennan, T., Kueh, A.J., and Thomas, T. (2012). Chromatin immunoprecipitation of mouse embryos. Methods Mol. Biol. *809*, 335–352. https://doi.org/10.1007/978-1-61779-376-9_23.

97. Ramírez, F., Ryan, D.P., Grüning, B., Bhardwaj, V., Kilpert, F., Richter, A.S., Heyne, S., Dündar, F., and Manke, T. (2016). deepTools2: a next generation web server for deep-sequencing data analysis. Nucleic Acids Res. *44*, W160–W165. https://doi.org/10.1093/nar/gkw257.

98. Yue, F., Cheng, Y., Breschi, A., Vierstra, J., Wu, W., Ryba, T., Sandstrom, R., Ma, Z., Davis, C., Pope, B.D., et al. (2014). A comparative encyclopedia of DNA elements in the mouse genome. Nature *515*, 355–364. https://doi.org/10.1038/nature13992.

99. Phipson, B., Lee, S., Majewski, I.J., Alexander, W.S., and Smyth, G.K. (2016). Robust hyperparameter estimation protects against hypervariable genes and improves power to detect differential expression. Ann. Appl. Stat. *10*, 946–963. https://doi.org/10.1214/16-aoas920.

STAR★METHODS

KEY RESOURCES TABLE

REAGENT or RESOURCE	SOURCE	IDENTIFIER
Antibodies		
anti-GFAP	Dako	Z0334
anti-nestin	Chemicon	MAB353
anti-SOX2	Millipore	AB5603
anti-H3S10p	Millipore	06,570
anti-H3K14ac	Upstate	070,353
anti-O4	Millipore	MAB345
anti-ßIII-tubulin	Promega	G7121
anti- O4-A594	R&D	FAB1326T
anti-ßIII-tubulin-PerCPCy5.5	R&D	IC1195C
anti- S100β	Abcam	Ab52642
anti- GFAP-A488 Clone GA5	Invitrogen	53-9892-82
anti- GFAP-Cy3	Abcam	Ab49874
anti- Sox2-APC	R&D	IC2018A
anti-TBR1 rabbit antibody	Abcam	ab31940
anti-CTIP2 rat antibody	Abcam	ab18465
anti-SATB2 mouse antibody	Abcam	ab51502
anti-BrdU antibody	Dako	M0744
anti-H4K5ac	Millipore	07-327
anti-H4K8ac	Millipore	07-328
anti-H4K16ac	Millipore	07-329
anti-H3K9ac	Millipore	07-352
anti-H3K14ac	Millipore	07-353
anti-H3K14ac	Cell Signaling	7627s
anti-H3K14ac	Abcam	ab52946
anti-H4K12ac	Abcam	AB1761
anti-KAT7	Protein Tech	13751-1-AP
anti- β-actin	Santa Cruz	sc-1616
anti-rabbit IgG HRP-conjugated	GE healthcare	NAV934v
Goat anti-Rabbit IgG (H + L) TRITC	Jackson Immunoresearch	111-0250993
Alexa Fluor 350 conjugated goat anti-rabbit antibody	Invitrogen	A21068
Alexa Fluor 488 conjugated goat anti-mouse antibody	Invitrogen	A11029
Alexa Fluor 546 conjugated goat anti-rat antibody	Invitrogen	A11081
Donkey anti-Rabbit DyLight 405 AffiniPure F(ab') Fragment	Jackson Immunoresearch	711-476-152
Alexa 546 goat anti-Rabbit	Invitrogen	A-11035
FITC-conjugated goat anti-mouse IgM	Vector Laboratories	FI2020
Alexa-Fluor 568-conjugated goat anti-mouse antibody	Invitrogen	A21124
AMCA-conjugated goat anti-rabbit antibody	Jackson ImmunoResearch	111-156-003
Vectastain Elite ABC Kit Universal	Vector Laboratories	PK6200
Biological samples		
Tissue samples isolated from the mice below	this study	N/A
Chemicals, peptides, and recombinant proteins		
LIVE/DEADTM fixable dye	ThermoFisher	L34955

(*Continued on next page*)

Continued		
REAGENT or RESOURCE	SOURCE	IDENTIFIER
FuGENE transfection reagent	Roche	11,814,443,001
Tissue-Tek O.C.T compound	ProSciTech	IA018
Dako fluorescence mounting medium	Agilent Dako	CS703
Critical commercial assays		
Apoptag fluorescein staining kit	Chemicon	S7160
Qiagen RNeasy kit	Qiagen	74,104
TruSeq library construction kit	Illumina	v2
Deposited data		
RNA-seq data (proliferating and differentiating *Kat7* intact and deleted NSPCs)	NCBI GEO	GSE215970
ChIP-seq data (H3K14ac on proliferating and differentiating wild-type NSPCs)	NCBI GEO	GSE215971
ChIP-seq data (H3K14ac and KAT7 occupancy on proliferating *Kat7* intact and deleted NSPCs)	NCBI GEO	GSE216459
Cortical neurons RNA-seq (on proliferating *Kat7* intact and deleted CN)	NCBI GEO	GSE220602
Neural stem cell RNA-seq (on proliferating *Kat7* intact and deleted NSPCs)	NCBI GEO	GSE220498
Experimental models: Cell lines		
Neural stem cells/neural stem and progenitor cells isolated from the mice below and cultured as neurospheres or differentiated	this study	N/A
Primary cortical neurons isolated from the mice below and cultured	this study	N/A
HEK293T cells for virus production	in house	N/A
Experimental models: Organisms/strains		
Kat7^{lox} mice	in house	(Kueh et al., 2011)[33]
NesCre$^{T/+}$ transgenic mice	Günther Schütz	(Tronche et al., 1999)[61]
Kat7$^{lox/+}$;*NesCre*$^{T/+}$ mice	bred from the two strains above, this study	N/A
Oligonucleotides		
Kat7 genotyping primers	in house:	N/A
TAAGAGCTATTCCGTGTTCCGG	(Kueh et al., 2011)[33]	oligonucleotide “1”
AACTGGAAATTCTTTGGCGCTCC	(Kueh et al., 2011)[33]	oligonucleotide “2”
ATCAATTCTGCCTGGCTTAACCC	(Kueh et al., 2011)[33]	oligonucleotide “3”
Recombinant DNA		
Kat7-pMIG (pMSCV-Kat7-IRES-GFP)	this study	N/A
pMSCV-IRES-GFP (pMIG)	Hilton lab, in house	N/A
gag/pol expression vector	Herold lab, in house	N/A
VSV-G expression vector	Herold lab, in house	N/A
Software and algorithms		
R	R Project for Statistical Computing	RRID:SCR_001905
R packages Rsubread, edgeR and limma	Bioconductor	RRID:SCR_006442
Mus musculus gene information	NCBI	ftp://ftp.ncbi.nlm.nih.gov
DAVID	david.ncifcrf.gov	RRID:SCR_001881
deepTools	https://deeptools.readthedocs.io/en/develop/	RRID:SCR_016366
Prism GraphPad Software	GraphPad	Version 9.4.1
STATA 17.0	StataCorp	Version 17.0

RESOURCE AVAILABILITY

Lead contact

Requests for further information and resources should be directed to and will be fulfilled by the lead contact Anne Voss (avoss@wehi.edu.au).

Materials availability

This study did not generate new unique reagents. We published the *Kat7* conditional mutant mouse strain previously.[33,35,36,45]

Data and code availability

- High-throughput sequencing data have been deposited at GEO and are publicly available. Accession numbers are listed in the key resources table. Western blot images (Data S1) and images of Ponceau S staining of histone Western blots (Data S2) are available in the Supplemental information.
- This paper does not report custom code.
- Any additional information required to reanalyze the data reported in this work paper is available from the lead contact upon request.

EXPERIMENTAL MODEL DETAILS

Mice

All animal experiments were conducted with approval of the WEHI Animal Ethics Committee and according to the Australian code for the care and use of animals for scientific purposes. We used our conditional mutant allele [*Kat7*^{lox}][33] to delete exon 1 of the mouse *Kat7* locus using cre-recombinase driven by the *nestin* intron 2 enhancer [*NesCre*$^{T/+}$ transgenic mice].[61] All mice were on a C57BL/6 inbred genetic background. Mice were kept in a 12 h light/12 h dark cycle. Noon of the day the vaginal copulation plug was first observed was defined as embryonic day 0.5 (E0.5). Mice were genotyped by genomic 3-way PCR[33] using the primers listed in the key resources table. To assess DNA replication rates during embryonic development, dams were administered a single pulse of BrdU by intraperitoneal injection at a dose of 100 μg/g at E14.5 and sacrificed after 1 h. Dissected embryonic brains were fixed in 4% PFA for future sectioning and staining.

Cortical neurons isolation, culture and viability stain

Cortical neurons were isolated from E16.5 cortices and cultured, as described previously.[76] In brief, E16.5 cerebral hemispheres were dissected, dissociated enzymatically and mechanically, passed through a sieve, collected by centrifugation and plated onto poly-L-lysine-coated tissue culture plates in neural differentiation medium [DMEM/F12, 5 mM HEPES, 13.4 mM NaHCO3, 0.6% D-glucose, 100 U/mL penicillin, 100 μg/mL streptomycin, 60 μM putrescine, 20 nM progesterone, 25 μg/mL insulin, 100 μg/mL apotransferrin, 30 nM selenium, 1% fetal bovine serum]. Cortical neuron viability was assessed at 24 h, 72 h and 120 h of culture using a live/dead assay kit (Molecular probes, L3224) according to manufacturer's instructions.

NSPC isolation, culture and differentiation

NSPC isolation, culture and differentiation were conducted as previously described.[77] In brief, E14.5 embryonic cortices and ganglionic eminences were dissected, washed in PBS, digested with pancreatin/trypsin, washed, resuspended in neurosphere culture medium [DMEM/F12, 5 mM HEPES, 13.4 mM NaHCO3, 0.6% D-glucose, 100 U/mL penicillin, 100 μg/mL streptomycin, 60 μM putrescine, 20 nM progesterone, 25 μg/mL insulin, 100 μg/mL apotransferrin, 30 nM selenium, 10 ng/mL bovine recombinant fibroblast growth factor 2 (FGF2), 4 μg/mL heparin-sodium salt, 20 ng/mL murine epidermal growth factor (EGF), 2 mg/mL BSA fraction V], sieved, plated and cultured at 37°C and 5% CO_2. Cells were passaged using Accutase (Sigma-Aldrich, A6964) for 5 min at 37°C to dissociate neurospheres and replated at 20,000 cells/cm^2. To determine short-term neurosphere proliferation rates, the mean diameter and spherical volumes of 20 randomly selected neurospheres per sample was measured on days 3, 6 and 9 during a single passage (passage 5) of culture. To determine neural stem cell long-term proliferation rates, neurospheres were passaged a total of 15 times over 105 days. To assess neurosphere self-renewal, neurospheres were passages and the number of secondary neurospheres forms was counted. To induce differentiation, neurospheres were dissociated and cultured on laminin substrate in cortical neuron culture medium.

METHOD DETAILS

NSPC immunofluorescence

For the detection of marker proteins, neurospheres were fixed in PFA, washed, permeabilized, blocked and incubated with intervening washing steps with the following antibodies: anti-GFAP (Dako, Z0334), anti-nestin (Chemicon, MAB353), anti-SOX2 (Millipore, AB5603), or anti-H3S10p (Millipore, 06,570), secondary antibodies and nuclear counter stain (Invitrogen, H1399). Differentiated

cultures were fixed with PFA, washed, blocked, and with intervening washing steps incubated with anti-O4 mouse antibody (Millipore, MAB345, washed in MT-PBS (2 × 10 min), FITC-conjugated goat anti-mouse IgM (Vector Laboratories, FI2020), anti-ßIII-tubulin mouse antibody (Promega, G7121) and anti-GFAP rabbit antibody (Dako, Z0334) with permeabilisation (0.25% Triton X-100), Alexa-Fluor 568-conjugated goat anti-mouse antibody (Invitrogen, A21124) and AMCA-conjugated goat anti-rabbit antibody (Jackson ImmunoResearch, 111-156-003).

NSPC flow cytometry

NSPCs were grown under proliferation or differentiating conditions as described above. Flow cytometry was conducted using the BD FACS Aria W (FACS Aria™ II SORP, BD Biosciences) cell analyser at a flow rate of less than 7,500 events/sec. Collected data were analyzed using FlowJo 10.1r5 (Tree Star Inc.).

For proliferation conditions, cells were collected by centrifugation (200 *g*, 5 min) and washed in MT-PBS (Gibco, 10,010,023). Cells were incubated at RT for 30 min with a LIVE/DEAD™ fixable dye (ThermoFisher, L34955). Cells were washed in MT-PBS and collected by centrifugation. Cells were fixed and permeabilised using eBioscience™ Intracellular fixation and permeabilization buffer set (ThermoFisher, 88-8824-00) for 1 h on ice. Cells were washed in 3 mL 2% FACS buffer (2% (vol/vol) FCS in FACS buffer: 150 mM NaCl, 3.7 mM KCl, 2.5 mM $CaCl_2 \cdot 2H_2O$, 1.2 mM $MgSO_4 \cdot 7H_2O$, 0.8 mM K_2HPO_4, 1.2 mM KH_2PO4, 11.5 mM HEPES) for 10 min on ice. Cells were collected by centrifugation (200 *g*, 5 min). Cells were incubated O/N at 4°C with primary or conjugated antibodies. The following morning cells were washed twice for 10 min with 2% FACS buffer. Cells were collected (200 *g*, 5 min) and incubated with secondary antibodies on ice for 1 h. Cells were washed twice for 10 min in 2% FACS buffer. Cells were resuspended in 2% FACS buffer and run on a FACS analyser.

For differentiation conditions, cells were collected by centrifugation (200 *g*, 5 min) and washed in 2% FACS buffer. Cells were stained for O4-A594 (R&D, FAB1326T) in 2% FACS buffer for 1 h on ice. Cells were washed in 3 mL FACS buffer and centrifuged (200 *g*, 5 min). Cells were fixed and permeabilised using eBioscience™ Intracellular fixation and permeabilization buffer set (ThermoFisher, 88-8824-00) for 1 h on ice. Cells were washed in 3 mL 2% FACS buffer for 10 min on ice. Cells were collected by centrifugation (200 *g*, 5 min) and incubated O/N at 4°C with primary or conjugated antibodies. The following morning cells were washed twice for 10 min in 2% FACS buffer, collected and incubated with secondary antibodies on ice for 1 h. Cells were washed twice for 10 min in 2% FACS buffer, collected and resuspended in 2% FACS buffer prior to analysis on a FACS analyser.

The following antibodies were used: O4-A594, R&D, FAB1326T; ßIII-tubulin-PerCPCy5.5, R&D, IC1195C; S100β, Abcam, Ab52642; GFAP-A488 Clone GA5, Invitrogen, 53-9892-82; GFAP-Cy3, Abcam, Ab49874; Sox2-APC, R&D, IC2018A; Donkey anti-Rabbit DyLight 405 AffiniPure F(ab') Fragment, Jackson Immunoresearch, 711-476-152; Alexa 546 goat anti-Rabbit, Invitrogen, A-11035.

Retroviral expression of Kat7 *in* pMIG

To produce *Kat7* overexpression virus particles, a transfection cocktail of 1 μg of *Kat7-pMIG (pMSCV-Kat7-IRES-GFP)* or empty vector *pMSCV-IRES-GFP (pMIG)*, 0.9 μg gag/pol and 0.1 μg VSV-G expression vectors were incubated in FuGENE transfection reagent (Roche, 11,814,443,001), before addition to HEK293T cells. After overnight culture, culture medium was replaced with fresh medium and viral supernatants were harvested 48 h later and filtered through a 0.45 μm syringe filter. 4 mL of viral supernatant with 8 μg/mL polybrene was added to dissociated neurospheres either during the first week after isolation (early transduction time point) or during week 5 after isolation (late transduction time point).

Immunofluorescence for cortical layer formation

Frozen cryosections were fixed in PFA, washed, permeabilised, blocked and incubated with intervening wash steps with anti-TBR1 rabbit antibody (Abcam, ab31940), anti-CTIP2 rat antibody (Abcam, ab18465) and anti-SATB2 mouse antibody (Abcam, ab51502), Alexa Fluor 350 conjugated goat anti-rabbit antibody (Invitrogen, A21068), Alexa Fluor 488 conjugated goat anti-mouse antibody (Invitrogen, A11029) and Alexa Fluor 546 conjugated goat anti-rat antibody (Invitrogen, A11081). For the enumeration of TBR1, CTIP2 and SATB2 positive cells of the E18.5 cortical plate on coronal sections, the fields of view were equally divided into 10 pial to ventricular bins and TBR1, CTIP2 and SATB2 positive cells were counted in each bin and presented as a percentage of total cells in the respective bins.

Immunofluorescence on E18 coronal brain sections

E18 fetuses were collected and euthanised by hypothermia on ice for 2 h. Heads were frozen in Tissue-Tek O.C.T compound (ProSciTech, IA018). 10 μm coronal sections were cut using a cryostat microm H550 (Thermo Fisher, 388,114) and placed onto SuperFrost Plus charged slides (Thermo Fisher, 4951PLUS4).

Selected slides were rehydrated in PBS (Gibco, 14,190,144). Sections were fixed in 1% PFA for 5 min at RT in a wet chamber, followed by 2 x PBS washes, 5 min each. Sections were permeabilised using 1% Triton X-100 for 30 min at RT in a wet chamber, 2 x PBS washes, 5 min. Non-specific staining was blocked using 10% FCS at RT for 30 min. Primary antibodies were added in 10% FCS in PBS, and sections were stained overnight at 4°C. The following morning sections were washed in PBS, 2 × 5 min and incubated with secondary antibodies in 10% FCS for 1 h at RT. Sections were washed, 2 × 5 min in PBS. Sections were incubated with DAPI in 10% FCS for 5 min at RT. Sections were washed, 2 x PBS, 5 min and mounted using Dako fluorescence mounting medium (Agilent Dako, CS703). Sections were photographed using a fluorescent microscope (Zeiss Axioplan 2).

The following antibodies were used: S100β, Abcam, Ab52642; GFAP-A488 Clone GA5, Invitrogen, 53-9892-82; Goat anti-Rabbit IgG (H + L) TRITC, Jackson Immunoresearch, 111-0250993.

BrdU immunohistochemistry

Paraffin sections were dewaxed, subjected to antigen unmasking solution (Vector, H3301), H_2O_2, washed, blocked and incubated with intervening wash steps with anti-BrdU antibody (Dako, M0744; 1:10 dilution) and Vectastain Elite ABC Kit Universal (Vector Laboratories, PK6200). BrdU positive cells were counted in at least 3 view fields of the developing cerebral cortex per sample on coronal sections of E14.5 brains.

TUNEL staining

TUNEL staining was conducted using an Apoptag fluorescein staining kit (Chemicon, S7160) according to manufacturer's instruction.

Radioactive *in situ* hybridisation

Radioactive in situ hybridisation was performed as previously described.[78] In brief, paraffin-embedded tissue sections were dewaxed, rehydrated through graded concentrations of alcohol, incubated for 10 min at room temperature in 10 mg/mL proteinase K, fixed in 4% paraformaldehyde for 10 min, then dehydrated through graded concentrations of alcohol. Sections were air dried, and hybridisation solution [300 mM NaCl, 5 mM EDTA•Na_2, 10 mM NaH_2PO_4•H_20, 10 mM Tris•Cl pH 6.8, 0.02% (w/v) polyvinylpyrrolidone, 0.02% (w/v) Ficoll 400, 0.02% (w/v) BSA fraction V (Sigma A-7906), 50% (v/v) formamide (deionised from IBI cat IB72020), 20% (v/v) dextran sulfate], containing 5×10^5 cts/min/μl *in vitro* transcribed with [S][35] labeled CTP, cRNA probes was placed over the section. Slides were incubated overnight at 56°C and then washed in 2xSSC [17.53 g/L NaCl,8.82 g/L sodium citrate, pH 7.0]/50% (v/v) formamide, 10 mM DTT at 60°C for 30 min and twice in 0.5 M NaCl, 10 mM Tris•Cl pH 8.0, 1 mM EDTA•Na_2 at 37°C for 5 min. Sections were incubated in 0.5 M NaCl, 10 mM Tris•Cl pH 8.0, 1 mM EDTA•Na_2 with 20 μg/mL RNase A at 37°C for 30 min, washed in 0.5 M NaCl, 10 mM Tris•Cl pH 8.0, 1 mM EDTA•Na_2 at 37°C for 30 min, washed twice in 2xSSC/50% (v/v) formamide at 60°C for 30 min, washed in 0.1xSSC at 60°C for 30 min, dehydrated through graded concentrations of alcohol and air dried for 1 h. Sections were exposed to an X-ray film, then coated in film emulsion (Kodak, NTB-2), exposed for 6 weeks, then developed (Kodak D19 developer), cleared in 30% sodium thiosulfate for 5 min, washed in distilled water, counterstained with haematoxylin, cover-slipped and photographed using darkfield optics (Axioplan 2 and Axiocam HR, Zeiss).

Protein lysis, acid protein extraction and immunoblotting

Cells were lysed in RIPA buffer (1% (v/v) Triton X-100, 0.1% (w/v) SDS, 1% (w/v) sodium deoxycholate, 150 mM NaCl, 10 mM Tris-HCl pH 7.5, 0.01% (w/v) sodium azide in Milli-Q H2O) with protease inhibitor (Roche, 05,892,791,001) for 30 min at 4°C.

For acid extraction of histones, cells were lysed in histone lysis buffer [10 mM HEPES pH 7.9, 1.5 mM MgCl2, 10 mM KCl, 0.5 mM DTT, 1.5 mM PMSF, 10 mM Na butyrate in Milli-Q H2O], HCl was added to tubes to a final concentration of 0.2 M, samples were incubated for 30 min on ice, centrifuged at 17,800 g, supernatants were transferred into dialysis tubing (Spectrum labs, 133,110) with a molecular weight cut-off of 3.5 kD, dialyzed against 500 mL of 0.1 M acetic acid (2 × 2 h), dialyzed against 500 mL of Milli-Q H2O for 1 h, 3h and overnight.

Protein lysates in SDS sample buffer [5x: 0.2 M Tris-HCl pH 6.8, 20% (v/v) glycerol, 10 mM β-mercaptoethanol, 0.05% (w/v) bromophenol blue in Milli-Q H2O] were incubated for 5 min at 95°C and separated by SDS-PAGE using 4-12% (w/v) Bis-Tris polyacrylamide gels (Invitrogen, NP0335PK2) at 145 V in MES running buffer (NP0002, Invitrogen) and transferred onto Osmonics PVDF membranes (Krackeler scientific, 243-1212639) using transfer equipment (BioRad, 170-3930) in Western transfer buffer (150 mM glycine, 20mM Tris, 20% (v/v) methanol in Milli-Q H2O) at 100 V for 2 h. Membranes were blocked in 10% (w/v) skim milk in PBST for 2 h at RT, washed in PBST (5 × 5 min), incubated with primary antibodies overnight in 5% (w/v) skim milk in PBST at 4°C, washed in PBST (5 × 5 min) and incubated with an anti-rabbit IgG HRP-conjugated secondary antibody (GE healthcare NAV934v) in 5% (w/v) skim milk in PBST at RT for 30 min. Protein bands were detected by incubating membranes in developing reagents (Millipore, WBKLS0100) for 2 min at RT before exposure to chemiluminescent film (GE healthcare, 28-9068-36).

Sample cohorts for RNA-seq and ChIP-seq experiments

Three RNA-seq and two ChIP-seq experimental series were conducted: a first cohort of samples of proliferating NSPCs was used to examine the effects of loss of KAT7 ($Kat7^{lox/lox}NesCre^{T/+}$ = *Kat7* deleted versus $Kat7^{+/+}NesCre^{T/+}$ = *Kat7* intact) with RNA-seq, KAT7-ChIP-seq and H3K14ac-ChIP-seq experiments and to assess a correlation between H3K14ac and mRNA levels (Figures 4A–4D, S7, S8 and Table S5); a second cohort of samples of proliferating and differentiating NSPCs were used to examine the effects of loss of KAT7 ($Kat7^{lox/lox}NesCre^{T/+}$ = *Kat7* deleted versus $Kat7^{+/+}NesCre^{T/+}$ = *Kat7* intact) on mRNA levels comparing proliferating and differentiating NSPCs and to assess a correlation between mRNA levels and H3K14ac levels (wild-type only) during differentiation (Figures 3, 4E–4G, S6, S9, Tables S1, S2, S3, S4, S6, and S7); the third cohort of samples were cortical neurons isolated at E16.5 and cultured overnight and were used to assess the effects of loss of KAT7 ($Kat7^{lox/lox}NesCre^{T/+}$ = *Kat7* deleted versus $Kat7^{+/+}NesCre^{T/+}$ = *Kat7* intact) on mRNA levels during neuronal development *in vivo* with RNA-seq (Figure 6, Tables S8 and S9).

RNA-seq profiling of cortical neurons

Sample cohort 3: Total RNA was isolated using Qiagen RNeasy kit (Qiagen, 74,104) according to the manufacturer's instructions from E16.5 cortical neurons isolated and cultured overnight. RNA was sent to BGI Beijing for library construction and 49 bp single-end sequencing. Reads were aligned to mouse genome mm9 using the Rsubread package 1.4.0[79] with >98% reads successfully mapped. Read counts were summarised at the gene level using the Rsubread's featureCounts function and Rsubread's in-built RefSeq annotation.[80] MDS plots indicated that the cortical neuron genotypes segregated well. Obsolete Entrez IDs and genes with <1 count per million in less than 3 samples were filtered out leaving 12,580 genes for further analysis. Library sizes were normalized by the trimmed mean of M-value (TMM) method.[81] Differentially expressed (DE) genes were identified using edgeR exact tests.[82,83] A total of 2,192 genes were downregulated and 1,876 upregulated with false discovery rate (FDR) < 0.05 in the *Kat7*$^{lox/lox}$*Nes-Cre*$^{Tg/+}$ cells. Gene set enrichment tests were conducted using ROAST[84,85] for the following gene sets: REST and CoREST target genes,[86] apoptosis genes,[87] cell adhesion genes (KEGG), neural crest stem cell genes,[88,89] embryonic stem cells, primitive ectoderm, transient neurogenic progenitors, committed neurogenic progenitors and mature neurons.[62] Gene ontology and KEGG analyses were conducted using DAVID.[90,91]

RNA-seq profiling of neural stem cells

Sample cohorts 1 and 2: Total RNA was isolated using Qiagen RNeasy kit according to the manufacturer's instructions from E14.5 neurospheres cultured in neural stem cell proliferation medium or differentiation medium. Libraries were constructed using the Illumina TruSeq library construction kit according to the manufacturer's instructions and sequenced on an Illumina HiSeq (cohort 1) or NextSeq sequencer (cohort 2) obtaining 100 bp single-end reads (cohort 1) or 75 bp paired-end reads (cohort 2). Reads were aligned to the mm10 mouse genome using Rsubread.[92] 85% and 80% of reads were successfully mapped for the two cohorts respectively. Read counts were summarised at the gene level using the featureCounts and Rsubread's in-built RefSeq annotation.[80] Gene annotation was downloaded from the NCBI (ftp://ftp.ncbi.nlm.nih.gov).

For the cohort 1 analysis, obsolete Entrez Gene Ids, mitochrondial genes and genes with <0.5 count per million in less than 4 samples were filtered out leaving 13,703 for further analysis. Library sizes were normalized by the TMM method. Counts were transformed to $\log_2$ counts per million by the voom method[84] and differentially expressed (DE) genes were identified by limma moderated t-tests[93] at FDR <0.05. Tissue gene annotation was conducted using DAVID.[90,91]

For the cohort 2 analysis, only protein-coding genes were retained in the analysis. Sex-linked genes (Xist and Y chromosome) and genes with gene-model, GenBank or Riken accessions as gene symbols were also removed. Expression filtering used edgeR's filterByExpr function with min.count = 5 leaving 13,742 genes for downstream analyses. Linear models were estimated using edgeR's voomLmFit function with sample weights.[94] Differential expression was assessed using TREAT t-tests with FDR = 0.05 relative to a fold-change theshold of 1.5.[95] Pathway analyses were conducted using limma's goana function.

ChIP-seq analysis

Sample cohorts 1 and 2: The antibodies used for ChIP were the anti-KAT7 antibody used in the Western blot in Figure 1A (13751-1-AP from Protein Tech) and anti-H3K14ac antibodies (7,627 from Cell Signaling) used in the Western blot in Figure 3A, or (Abcam ab52946). 10 million cells per sample were used. Chromatin immunoprecipitation (ChIP) was conducted as reported previously;[96] libraries were generated using an Illumina TruSeq DNA library preparation kit and sequenced on an Illumina HiSeq (cohort 1) or NextSeq sequencer (cohort 2).

For cohort 1 analyses, ChIP-seq reads were aligned to mm10 using Bowtie2 aligner. The ChIP-seq libraries were GC corrected using Benjamini's and Speed's method implemented by the deepTools program.[97] The same number of *Kat7* deleted and intact cells per sample were used. ChIP-seq library read depth was normalised to cell number to enable detection of global differences in KAT7 occupancy and H3K14ac. Based on the Western blots (Figures 1A and 3A), KAT7 and H3K14ac reads were expected to be very low in *Kat7* deleted samples, which was also reflected in the very low DNA yield after ChIP (Figure S7). ChIP-seq libraries were converted to coverage files using non overlapping 100 bp bins. Using deepTools normalisation, the coverage was standardised to 1x depth. With this method the sequencing depth is computed as: (total number of mapped reads * fragment length)/effective genome size. The scaling factor used is the inverse of the sequencing depth computed for the sample to match the 1x coverage. For the plotting of localised areas, 10 base bins (default) were used (deepTools). ChIP-Seq gene counts were used for Figure S7G, and ChIP-Seq genome-wide 1 kb bin counts were used for Figure 4C. The following genomic features were used apart from genes with NCBI mm10 coordinate annotation. Promoter region was defined as −2 kb to ±0 relative to the TSS, post TES as TES ±0 to +2 kb. Pseudogenes and CpG islands bed files for the mm10 build were downloaded from the UCSC Genome Browser. To distinguish between CpG islands near to and far from the TSS a 10 kb threshold was chosen. The chromatin marks H3K27ac and DNase I hypersensitivity in the E14.5 forebrain were used to define enhancers. The result of combining these two marks was provided for mm10 by ENCODE [[98]; GSE82598 for H3K27ac (Bing Ren, UCSD); GSE83172 for DNase I hypersensitivity (John Stamatoyannopoulos, UW), combined as ENCSR337EDG_ENCSR320EEW_predictions.bed downloaded from the Weng laboratory website (Zhiping Weng, UMass)]. This definition will only reveal active enhancers. To distinguish between enhancers near to and far from the TSS a 12 kb threshold was chosen. The definition of origins of replication was taken from high-throughput sequencing data in mouse ES cells [[59]; GSE68347, three replicates plus control]. To distinguish between IS near and far from TSS a 10 kb threshold was chosen.

To assess heterochromatic regions of the genome, H3K9me3-ChIPseq neural progenitor cell data [[60]; GSM1375164; 2 replicates] were used to define broad peaks of H3K9me3 as described in the original publication.

For cohort 2 analyses, reads were aligned to the mm10 mouse reference genome using Rsubread.[92] Counts were assessed in two genomic regions: TSS to +1 kb downstream of the TSS and gene bodies using Rsubread's promoterRegion function and inbuilt RefSeq annotation. Only annotated protein-coding genes were retained as for the RNA-seq analysis described above. No expression filtering was done leaving 19,683 genes in the analysis. Library sizes were normalized by the TMM method with singleton pairing. Linear models were fitted using edgeR's voomLmFit function with the cell-types as variance groups.[94] Differential binding was assessed using robust empirical Bayes with FDR = 0.05.[99]

QUANTIFICATION AND STATISTICAL ANALYSIS

High-throughput sequencing data were analyzed as stated in detail in the RNA-seq and ChIP-seq method sections above. Otherwise, data were analyzed using Prism GraphPad Software Version 9.4.1 (458) or STATA 17.0 StataCorp to perform the tests stated in the Figure legends.